Available online at www.sciencedirect.com

SCIENCE DIRECT®

Lithos 83 (2005) 394–419

LITHOS

www.elsevier.com/locate/lithos

Partitioning coefficients between olivine and silicate melts

J.H. Bédard*

Geological Survey of Canada, RNCAN, 880 Ch.St.Foy, Québec, PQ, Canada G1S 2L2

Received 1 October 2003; accepted 18 February 2005
Available online 22 April 2005

Abstract

Variation of Nernst partition coefficients (D) between olivine and silicate melts cannot be neglected when modeling partial melting and fractional crystallization. Published natural and experimental $^{olivine/liquid}D$ data were examined for covariation with pressure, temperature, olivine forsterite content, and melt SiO_2, H_2O, MgO and MgO/MgO+FeO^{total}. Values of $^{olivine/liquid}D$ generally increase with decreasing temperature and melt MgO content, and with increasing melt SiO_2 content, but generally show poor correlations with other variables. Multi-element $^{olivine/liquid}D$ profiles calculated from regressions of D REE–Sc–Y vs. melt MgO content are compared to results of the Lattice Strain Model to link melt MgO and: D_0 (the strain compensated partition coefficient), E_M^{3+} (Young's Modulus), and r_0 (the size of the M site). Ln D_0 varies linearly with Ln MgO in the melt; E_M^{3+} varies linearly with melt MgO, with a dog-leg at ca. 1.5% MgO; and r_0 remains constant at 0.807 Å. These equations are then used to calculate $^{olivine/liquid}D$ for these elements using the Lattice Strain Model. These empirical parameterizations of $^{olivine/liquid}D$ variations yield results comparable to experimental or natural partitioning data, and can easily be integrated into existing trace element modeling algorithms. The $^{olivine/liquid}D$ data suggest that basaltic melts in equilibrium with pure olivine may acquire small negative Ta–Hf–Zr–Ti anomalies, but that negative Nb anomalies are unlikely to develop. Misfits between results of the Lattice Strain Model and most light rare earth and large ion lithophile partitioning data suggest that kinetic effects may limit the lower value of D for extremely incompatible elements in natural situations characterized by high cooling/crystallization rates.

Keywords: Partitioning; Olivine; Trace elements; Petrogenesis; Modeling

1. Introduction

1.1. Olivine and D

The Nernst partition coefficient 'D' is the ratio of the concentration of a trace element in a solid phase divided by its concentration in the equilibrium liquid, and is used extensively to model magmatic processes (e.g. Shaw, 1970, 2000; O'Hara, 1977, 1995; Hofmann, 1988; Langmuir, 1989; Bodinier et al., 1990; Bédard, 1994, 1999, 2001; Spera and Bohrson, 2002; Niu et al., 2002; Weyer et al., 2003; Maclennan et al., 2003). Uncertainties with regard to values of D are a major source of uncertainty in modeling crystal/liquid fractionation or melting, and in applying inversion

* Tel.: +1 418 654 2671; fax: +1 418 654 2615.
E-mail address: jbedard@rncan.gc.ca.

0024-4937/$ - see front matter © 2005 Elsevier B.V. All rights reserved.
doi:10.1016/j.lithos.2005.03.011

models to cumulates and mantle melting residues (Bédard, 1994, 2001). Olivine: is the most common upper mantle phase on Earth (e.g. Nixon, 1987) and other terrestrial planets and planetisimals (e.g. Barrat et al., 2002; Hsu, 2003; Karner et al., 2003); is an important cumulus phase in many intrusions, ophiolites and the lower oceanic crust (Cawthorn, 1996; Dilek and Robinson, 2003); crystallizes from a wide diversity of melts, including komatiite, basalt, ferrobasalt, and high-temperature granites and syenites (e.g. Barker et al., 1975; Arndt, 1977; Bédard et al., 1987; Grove and Juster, 1989; Blatter and Carmichael, 2001); and may play a role in generating the depletions in high field strength cations (HFSC: Ti, Zr, Ta, Nb) thought characteristic of arc environments (e.g. Kelemen et al., 1990). However, despite olivine's petrogenetic importance, relatively few data on $^{olivine/liquid}D$ are available, and these data show wide ranges in value. It is now widely accepted that $^{mineral/liquid}D$ are variable (e.g. Mysen and Virgo, 1980; Blundy and Wood, 1994b; Gaetani and Grove, 1995; Hill et al., 2000), but there have been few attempts to constrain how $^{olivine/liquid}D$ varies. The purpose of this paper is to provide an objective parameterization of the dominant trend of variation of D values that can be used to model igneous processes in common magmatic suites.

1.2. Data sources

All experimental and natural mineral/melt partitioning studies for which essential data were published or could be recovered from the authors were compiled, and are available as Supplementary data in the Appendix. Table 1 gives data sources and the corresponding letter/number acronyms that appear in some figures. Partitioning data originating from analysis of phenocrysts in lavas or intrusions are referred to as 'natural' data, and have a number code, while experimental partitioning data are given a letter code. Mineral/mineral partitioning studies were not considered because of subsolidus reequilibration effects (e.g. McDonough et al., 1992; Loucks, 1996). Information on partitioning of Ti, Cr, Na, Al and K was also gleaned from phase equilibrium studies. By considering these data together, it may be possible to unravel the causes of $^{olivine/liquid}D$ variations, and to express them quantitatively. For simplicity, sub/superscripts will be left out henceforth,

Table 1
Data sources

Experimental data
a=Elkins-Tanton and Grove, 2003
b=Brenan et al., 2003
c=Canil, 1997
d=Walter, 1998
e=Beattie, 1993
f=Toplis and Carroll, 1996
g=Baker and Eggler, 1987
h=Longhi, 1995
i=Kinzler and Grove, 1992
j=McDade et al., 2003
k=Elkins-Tanton et al., 2000, 2003 and personal communication 2003
m,M=McKay, 1986, Mare and LKFM
n=Moore and Carmichael, 1998
o=Colson et al., 1988
p=Parman and Grove, 2004
q=Baker and Stolper, 1994
r=Blatter and Carmichael, 2001
s=Kohn and Schofield, 1994
t=Righter and Carmichael, 1996
u=Purton et al., 2000
v=Scaillet and MacDonald, 2001
w=Wasylenki et al., 2003
x=Berndt, 2002
y=Mysen, 1978
z=Schwab and Johnson, 2001
A=Hanson and Jones, 1998
B=Shimizu et al., 1982
C=Pickering-Witter and Johnston, 2000
Ca=Capobianco et al., 1991
D=Dunn, 1987
Du=Duke, 1976
E=Canil and Fedortchouk, 2001
F=Grove and Juster, 1989
G=Nielsen et al., 1992
H=Longhi et al., 1999
I=Righter et al., 2004
J=Beattie, 1994
K=Kennedy et al., 1993
L=Kelemen et al., 1990
La=Laporte et al., 2004
N=Gaetani and Grove, 1998
Ne=Nekvasil et al., 2004
O=Hesse and Grove, 2003
P=Parman et al., 1997
Q=Longhi, 2002
R=Kinzler, 1997
S=Grove et al., 1982
Sc=Schmidt et al., 2004
T=Toplis et al., 1994
U=Adam and Green, personal communication, 2003
V=Grove et al., 2003

(continued on next page)

Table 1 (*continued*)

Experimental data
W=Sweeney et al., 1995
Y=Yang et al., 1996
Z=Herzberg and Zhang, 1996
Natural data
1=Dostal et al., 1983
2=Schnetzler and Philpotts, 1970
3=Brunet and Chazot, 2001
4=Mahood and Stimac, 1990
5=Mahood and Hildreth, 1983
6=Dunn and Sen, 1994
7=Francalanci, 1989
8=Dostal and Capedri, 1975
9=LeMarchand et al., 1987
10=Larsen, 1979
11=Villemant et al., 1980
12=Luhr and Carmichael, 1980
13=Fujimaki et al., 1984
14=Wörner et al., 1983
15=Shimizu et al., 1982
16=Burton et al., 2002
17=Puchtel et al., 2004

The letter and number codes are used in figures.

with the understanding that 'D' will always refer to $^{\text{olivine/liquid}}D$; e.g. $^{\text{olivine/liquid}}D_{\text{Sc}}=D$ Sc.

1.3. Choice of input parameter

What should be the input variable for the parameterization? The ability to reproduce the data is the main criterion, but ease of application must also be considered. It has been proposed that the composition of the melt is the main control on D variations, and attempts have been made to parameterize D variations against complex functions of melt chemistry, typically involving ratios of network-forming and network-modifying cations and anions (e.g. Nielsen and Drake, 1979; Mysen, 1983; Nielsen, 1985; Hanson and Jones, 1998; Colson et al., 2000). Two inherent problems with this approach are that some cations (Al^{3+}, Fe^{3+}, Ti^{4+}, P^{5+}) can fulfill different structural roles, and that the influence of volatile species is poorly constrained. Furthermore, to be accurate, these complex functions require that the melt composition be known exactly. While this applies to well-constrained experimental situations where equilibrium glasses can be analyzed; unaltered glass is rarely present in most pre-Mesozoic lavas, and so melt composition must equated with the whole-rock analysis, or be calculated. In addition, some elements (CaO, Na_2 O, K_2 O, SiO_2) are easily remobilized by hydrothermal alteration and metamorphism; and, when looking at cumulate or mantle rocks, it is rarely possible to know exactly the original temperature, pressure and melt composition at and from which the crystals formed. Consequently, simpler indices of melt compositional evolution are considered here, the values of which can be: (a) constrained empirically from lava or glass analyses; (b) calculated from the mineral analysis itself (e.g. MgO or MgO#=MgO/MgO+FeO total) through the application of exchange and distribution coefficients (e.g. Roeder and Emslie, 1970; Sugawara, 2000; Maclennan et al., 2003); or in the case of SiO_2, (c) calculated with a thermodynamic approach (e.g. Carmichael et al., 1970). Other investigators have favoured a mineral-compositional control on D variations, since distortions of the crystal structure resulting from solid-solutions are known to affect the size of the site(s) into which trace elements enter (e.g. Blundy and Wood, 1991, 2003; Gaetani and Grove, 1995). The mineral-compositional parameter considered in this paper is the molar forsterite content ($Fo=100\times Mg/Mg+Fe^{total}$) which is interlinked with liquid FeO/MgO (Roeder and Emslie, 1970).

1.4. Sources of error and uncertainty

This is a compilation of data from both experimental and natural partitioning studies, which were analyzed over a span of 25 years with different methods in different laboratories; so that one has to consider the probability of inter-laboratory biases, the progressive improvements in precision and accuracy that have occurred, the possibility that kinetic or pneumatolytic effects may have perturbed some experiments or observations, and finally, the probability of occasional experimental or typographical errors. Partitioning data obtained from phenocryst/matrix pairs are not as well constrained as experimental data because: (a) D is commonly calculated assuming that the matrix or bulk composition represents the liquid composition, (b) equilibrium may not always obtain, and (c) the potential effects of mineral or melt inclusions in mineral separates are not always considered. Nevertheless, these 'natural' partitioning values are also considered here because there are no

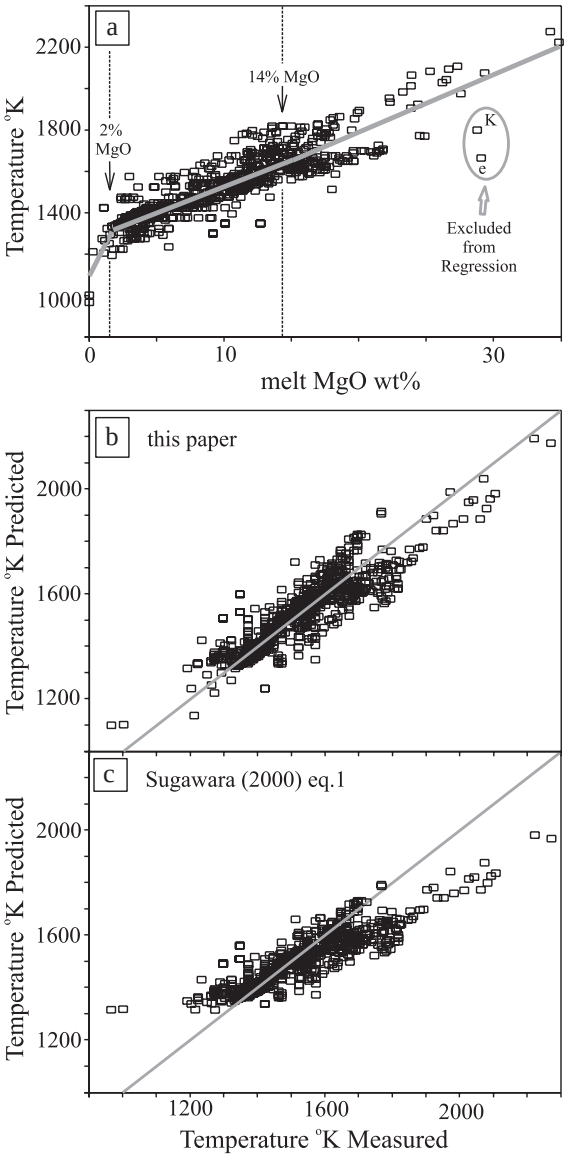

Fig. 1. (a) Experimental temperature in °K vs. melt MgO wt.% for the data compiled here. The data were regressed as three segments (0–2, 2–14 and >14 wt.% MgO), shown as thick grey lines (Table 2). Two datapoints were excluded from the high-MgO regression. (b and c) Comparison of measured temperatures with (b) temperatures calculated from the experimental MgO of the liquid using the regressions of Table 2, and (c) with Eq. (1) of Sugawara (2000).

experimental data available for some elements and melt compositional ranges. A potential problem with partitioning data obtained from phase equilibrium studies (Ti, Cr, Na, Al, K) is that olivine minor element analyses may not have been controlled as carefully as in the dedicated partitioning studies.

When analyzing the partitioning data, discrepant datapoints were excluded from some regressions. These exclusions are discussed below on a case-by-case basis. While discrepant data that result from experimental errors can safely be neglected, data outliers could reflect systematic differences in pressure, f_{O_2}, volatile activity, bulk composition, crystal chemistry..., etc. These alternatives were investigated where the database was adequate, but it was not always possible to determine why some datapoints or datasets were discrepant.

1.5. Approach

Because TiO_2 is easily analyzed with the electron microprobe, the *D* Ti dataset is large enough to allow

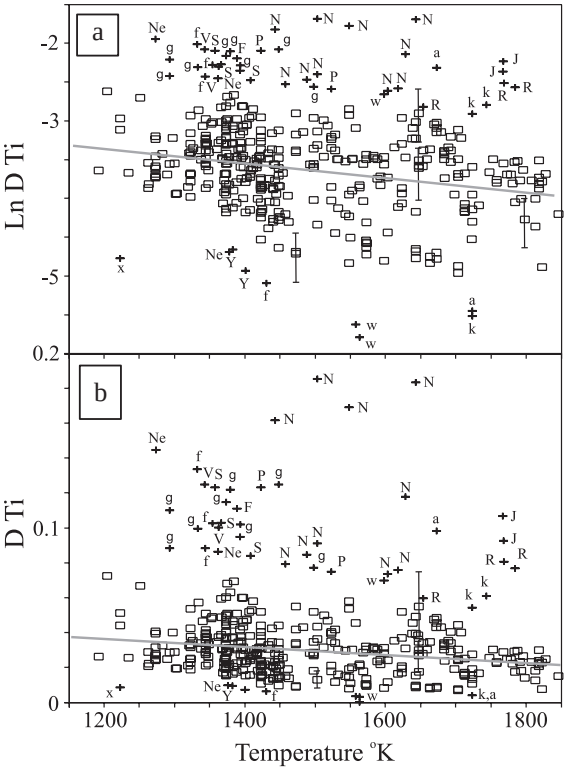

Fig. 2. (a) Ln *D* Ti and (b) *D* Ti vs. Temperature in °K. Crosses are discrepant data from this figure, and the letter and number codes are from Table 1. The thick grey lines are regressions (Table 2). Representative error estimates from some of the partitioning studies are shown.

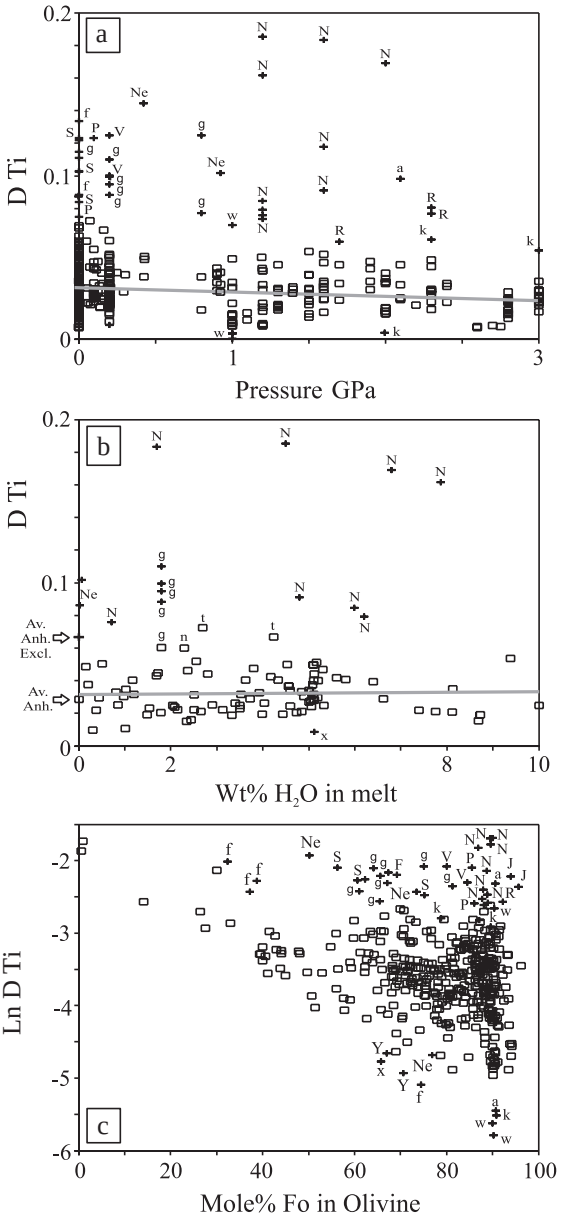

Fig. 3. (a) *D* Ti vs. Pressure in GPa, (b) *D* Ti vs. H_2O wt.% in melt, and (c) Ln *D* Ti vs. mol% Forsterite content of olivine. Crosses are discrepant data from Fig. 2, and the letter and number codes are from Table 1. The cross marked 'Av.Anh.Excl.' is the average of excluded anhydrous data; while the box marked 'Av.Anh.' is the average of anhydrous data included in the regression, and weighted as if it represented 10 datapoints. The thick grey lines are regressions (Table 2).

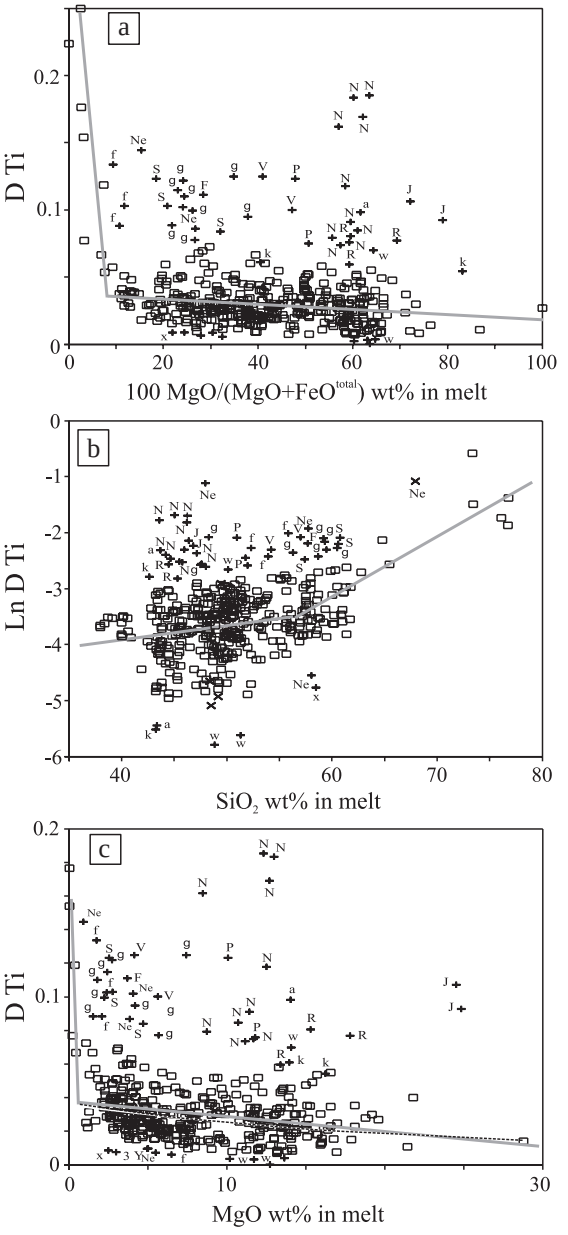

Fig. 4. (a) *D* Ti vs. 100MgO/(MgO+FeO^{total}) wt.% in melt, (b) Ln *D* Ti vs. SiO_2 wt.% in melt, and (c) *D* Ti vs. MgO wt.% in melt. Crosses are discrepant data from Fig. 2, and the letter and number codes are from Table 1. In 'b' some of the discrepant data were included in the regression, and these are marked as '×'. The thick grey lines are regressions (Table 2). In 'c' the preferred regression of Ln *D* Ti vs. MgO is shown as a heavy dotted line.

some of the causal mechanisms to be deduced (Figs. 1–4), and to determine the optimal input variable against which to parameterize *D* variations. A similar

exercise carried out for other elements showed similar systematics (e.g. *D* Sc, Fig. 5). Afterwards, most partitioning data will be regressed against the same variable (Figs. 6–12, Table 2). Elements for which insufficient partitioning data were available to allow regression were averaged (Table 2). Comparisons of the regression results for *D* REE–Y–Sc (Table 2) with the Lattice Strain Model of Blundy and Wood (1994a,b) are then used to derive equations linking MgO with D_0 (the strain compensated partition coefficient), *E* (Young's Modulus), and r_0 (the size of the M site) (Figs. 13 and 14, Table 3). From these equations (Table 3), values of *D* REE–Y–Sc can be calculated with the Lattice Strain Model, generating a composite parameterization that is consistent with theory, which can easily be integrated into existing spreadsheets and modeling algorithms, and that applies to a wide range of melt compositions (Fig. 15).

This simple and partly empirical approach is not meant as a substitute for thermodynamically based partitioning models (e.g. Beattie et al., 1991; Blundy et al., 1996; Colson et al., 2000; O'Neill and Eggins, 2002). Yet, despite considerable progress in developing such models (see Blundy and Wood (2003) for an overview), it is not yet possible to obtain the values of *D* for all elements and *P–T–X* conditions of interest in this way, and realistically, it will be many years before this becomes possible. For those needing a set of *D* values to model a given magmatic suite, a commonly used, commonsense approach has been to choose a set of *D* values from an experiment done at appropriate *P–T* conditions on a melt composition that is 'similar'

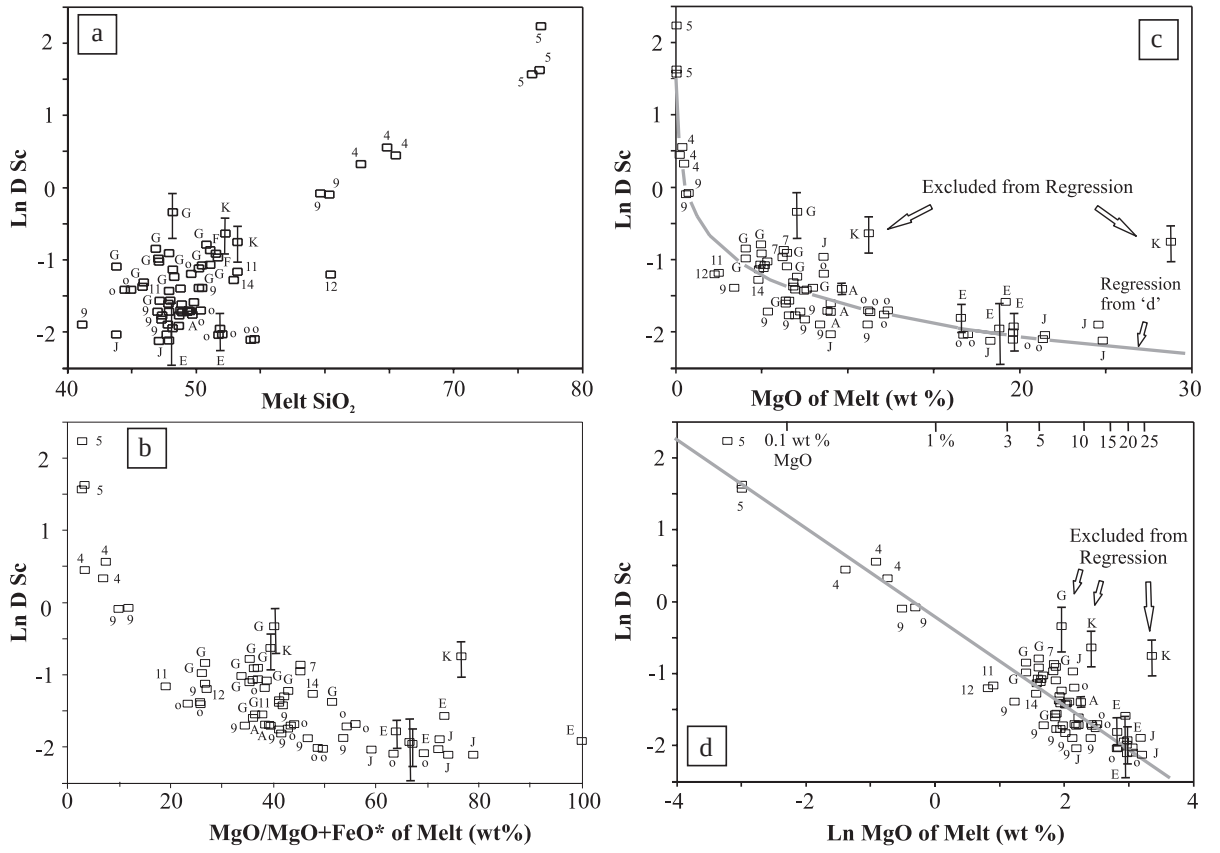

Fig. 5. Ln *D* Sc data (*D* Sc). Some data are annotated by letter or number codes (see Table 1 for key) and show representative error estimates. Data are plotted vs.: (a) melt SiO_2, (b) melt MgO/MgO+FeO^{total} (wt.%), (c) melt MgO (wt.%) and (d) Ln MgO (wt.%) in the melt. The thick grey line in 'c' and 'd' are regressions (Table 2).

to the suite being investigated. However: (a) few bulk compositions have been investigated in enough detail to do this; (b) few partitioning studies consider the entire geochemical spectrum, handicapping users of multi-element plots (e.g. Thompson et al., 1983); and (c) the variation of D's with changing P–T–X conditions would still not be accounted for. Given the need for a systematic, quantitative, multi-element estimate of $^{\text{olivine/liquid}}D$, and for how these D's vary, the partly empirical parameterization proposed here may furnish an interim, practical solution.

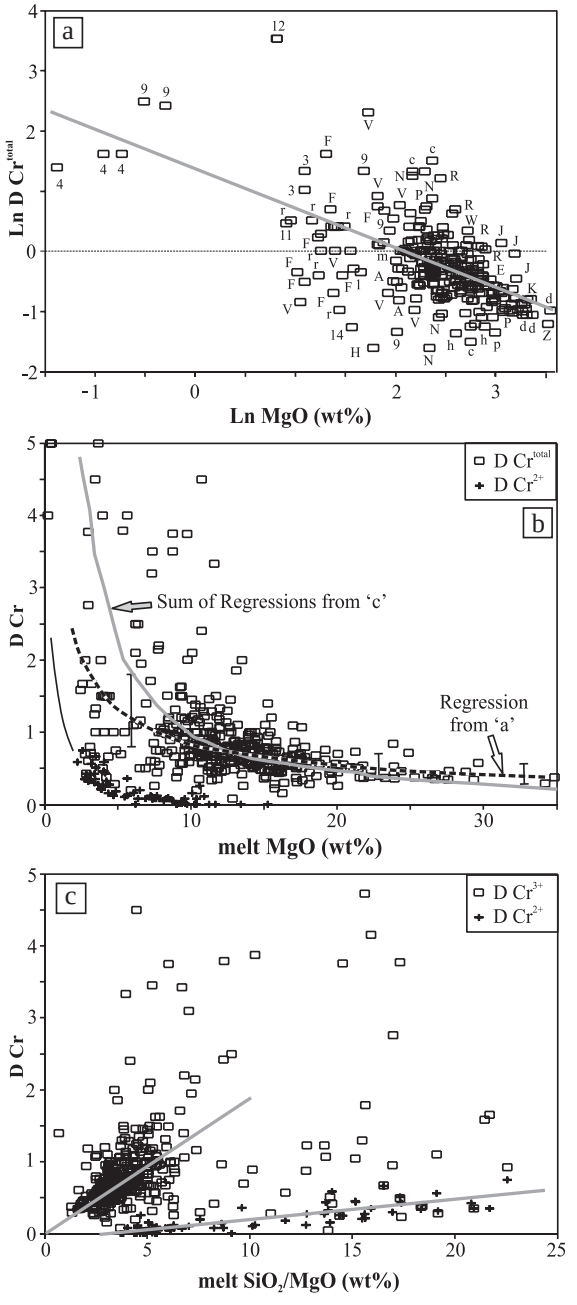

Fig. 6. (a) Ln D Cr^{total} vs. Ln MgO (wt.%) in melt. Thick grey line is a regression against all of the data (Table 2). (b) D Cr^{total} and D Cr^{2+} vs. MgO (wt.%) in melt. Values of D Cr^{2+} were calculated as proposed by Hanson and Jones (1998, Table 2), with a low-MgO extension marked in schematically. For MgO>5%, values of D Cr^{2+} are small. The heavy dotted line with error bars shows the value of D Cr^{total} calculated from the regression of 'a' (Table 2); and is very similar to the thick grey line, which shows the trend of the sum of the values of D Cr^{3+} and D Cr^{2+} calculated from the regressions of 'c' (Table 2). Note that these two parameterizations are very similar for MgO>5%. (c) D Cr^{3+} and D Cr^{2+} vs. SiO_2/MgO (wt.%) in melt. Values of D Cr^{2+} were calculated as in 'b', with D Cr^{3+}=D Cr^{total}−D Cr^{2+}.

2. Variations of $^{\text{olivine/liquid}}D_{\text{Ti}}$ (D Ti)

2.1. Temperature, pressure, and H_2O

2.1.1. Temperature–MgO

Temperature and melt MgO content are closely linked (Fig. 1). The data were regressed as three segments (0–2%, 2–14%, +14% MgO) to quantify variations of liquid MgO vs. temperature (Table 2). The equations will be used to link liquid MgO and temperature when applying the Lattice Strain Model (see below).

2.1.2. Temperature–D Ti

There is a diffuse trend of increasing D Ti with decreasing temperature for ultramafic, mafic and intermediate melt compositions (Fig. 2). Data from two low-temperature rhyolites from Scaillet and MacDonald (2001) have significantly higher D Ti and plot above this trend. A number of data that plot above or below the main trend are shown as crosses on Fig. 2. These anomalous datapoints are also shown as crosses in the next figures (Figs. 3 and 4), emphasizing the fact that the anomalous D Ti data are not unusual in terms of temperature, pressure, f_{O_2} conditions, or melt composition (including H_2O). Some of the very low D Ti data may represent TiO_2

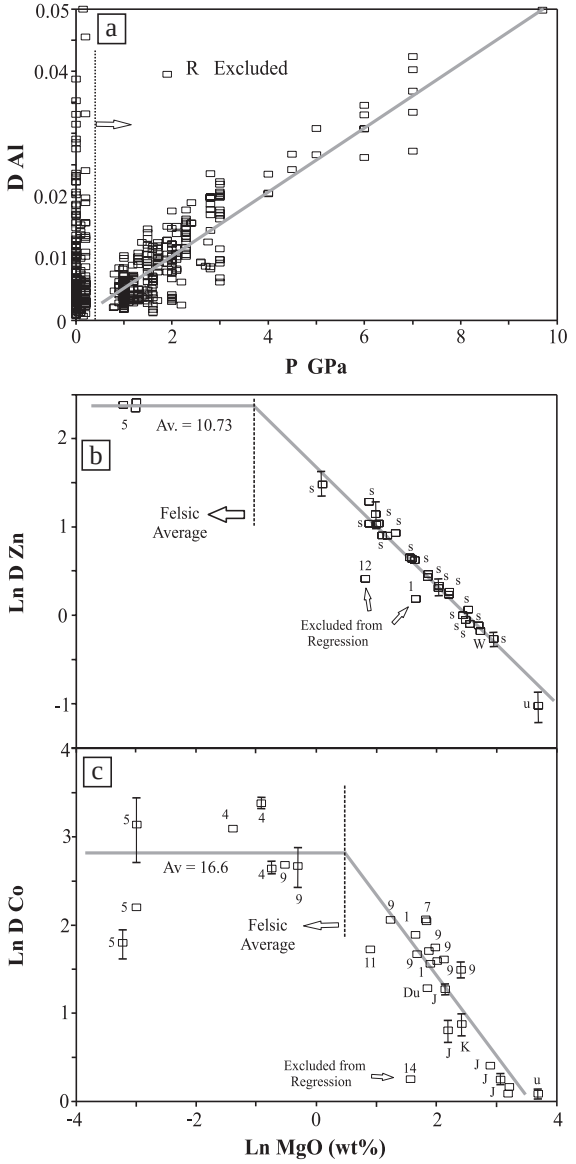

Fig. 7. (a) Ln *D* Al vs. Pressure in GPa, (b) Ln *D* Zn, and (c) Ln *D* Co vs. Ln MgO (wt.%). Thick grey lines are regressions or averages (Table 2).

detection problems: e.g. TiO_2 in olivine from runs #12 and #27C of Wasylenki et al. (2003, 'w') were 0.00125 and 0.000001 wt.%, respectively. The numerous high *D* Ti outliers constitute a more difficult problem. For example, consider experimental runs B304 and B333 of Gaetani and Grove (1998, 'N'). Although these two runs are virtually indistinguishable in terms of melt composition, were equilibrated at similar *P*, *T*, f_{O_2} conditions, with similar melt H_2O contents; run B304 yields a *D* Ti of 0.085 (discrepant), while run B333 yields a *D* Ti of 0.033 (concordant). Since no obvious reason could be established for the anomalous *D* Ti of most outliers, I infer that they may reflect systematic analytical biases or experimental errors, and so excluded them from the *D* Ti regressions.

2.1.3. Pressure–D Ti

When all of the mafic *D* Ti data (>1% MgO liquids) are considered together, a very shallow trend of *D* Ti increase with pressure decrease is observed (Fig. 3a). However, errors on this regression are large and the correlation coefficient is low (Table 2), suggesting that any influence of pressure on *D* Ti is probably overshadowed by other effects.

2.1.4. H_2O–D Ti

Recent work (Wood and Blundy, 2002) implies that differences in melt volatile contents affect clinopyroxene *D* values, and a similar effect might be suspected for olivine. However, olivine *D* Ti data show only a diffuse and shallow rate of increase vs. the H_2O content of the melt (Fig. 3b); suggesting that any effect that melt H_2O content may have is probably drowned out by other factors.

2.2. Mineral–chemical controls ($Fo = 100 \times Mg/Mg + Fe^{total}$)

Plots of *D* Ti against the Fo-content of olivine (Fig. 3c) show considerable scatter, and no regression was attempted. An additional complication is that olivine Fo-content and partitioning behaviour may be perturbed by sub-liquidus exchanges with other minerals (chromite or sulphide: e.g. Bédard and Hébert, 1998; Li et al., 2003), or evolved interstitial melt (Barnes, 1986).

2.3. Melt compositional controls (MgO#, SiO_2, MgO)

2.3.1. MgO# ($100MgO/(MgO + FeO^{total})$)

Values of *D* Ti increase gradually with decreasing MgO# for mafic melts, with a steeper increase in felsic melts (Fig. 4a). The trends of increase vs. MgO# are poorly defined, however. The data were regressed

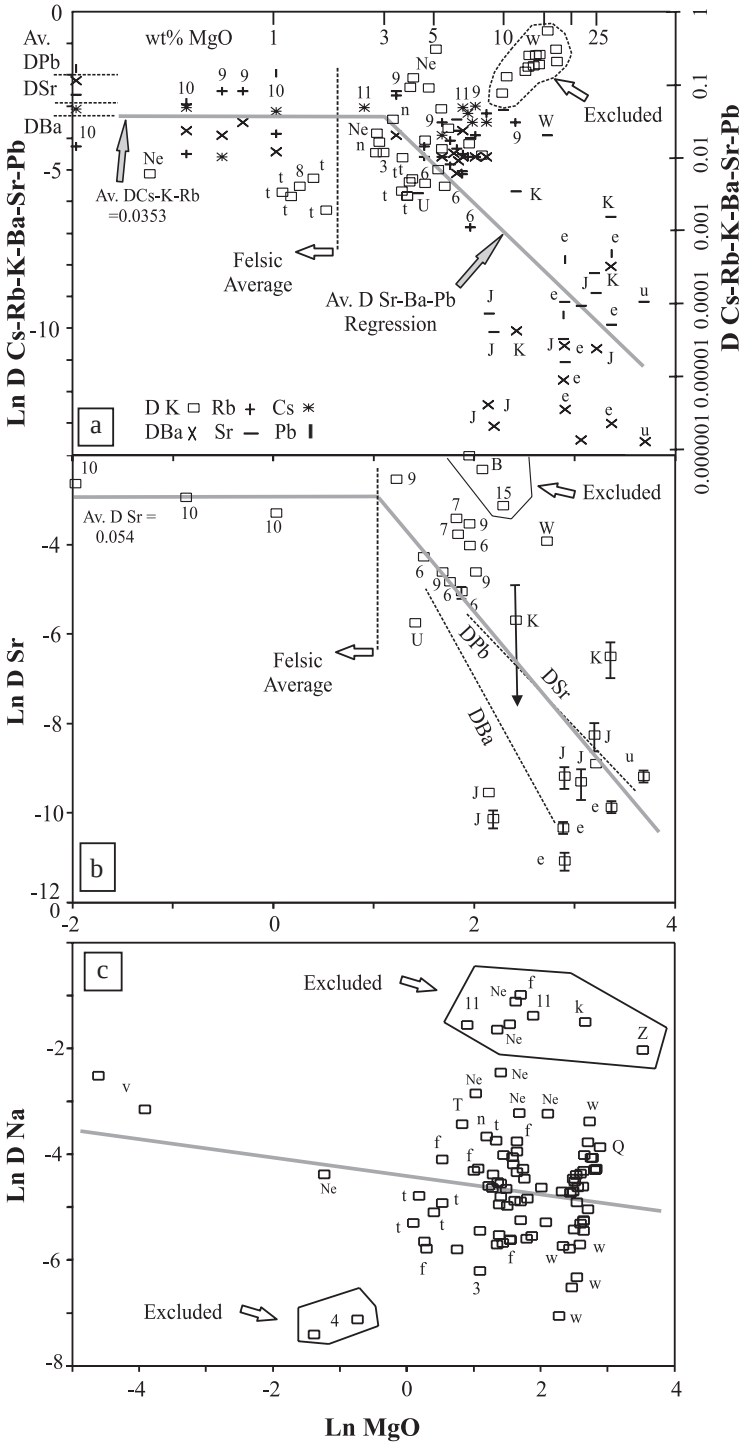

Fig. 8. (a) Ln *D* (Sr, Ba, Rb, Cs, K, Pb), (b) Ln *D* Sr, (c) Ln *D* Na vs. Ln MgO (wt.%). Representative error estimates for some data, and mafic–ultramafic regressions for *D* Ba and *D* Pb, are shown in 'b'. Linear equivalents for MgO and *D* data are shown for comparison in 'a'. Thick grey and dotted lines are regressions or averages from Table 2.

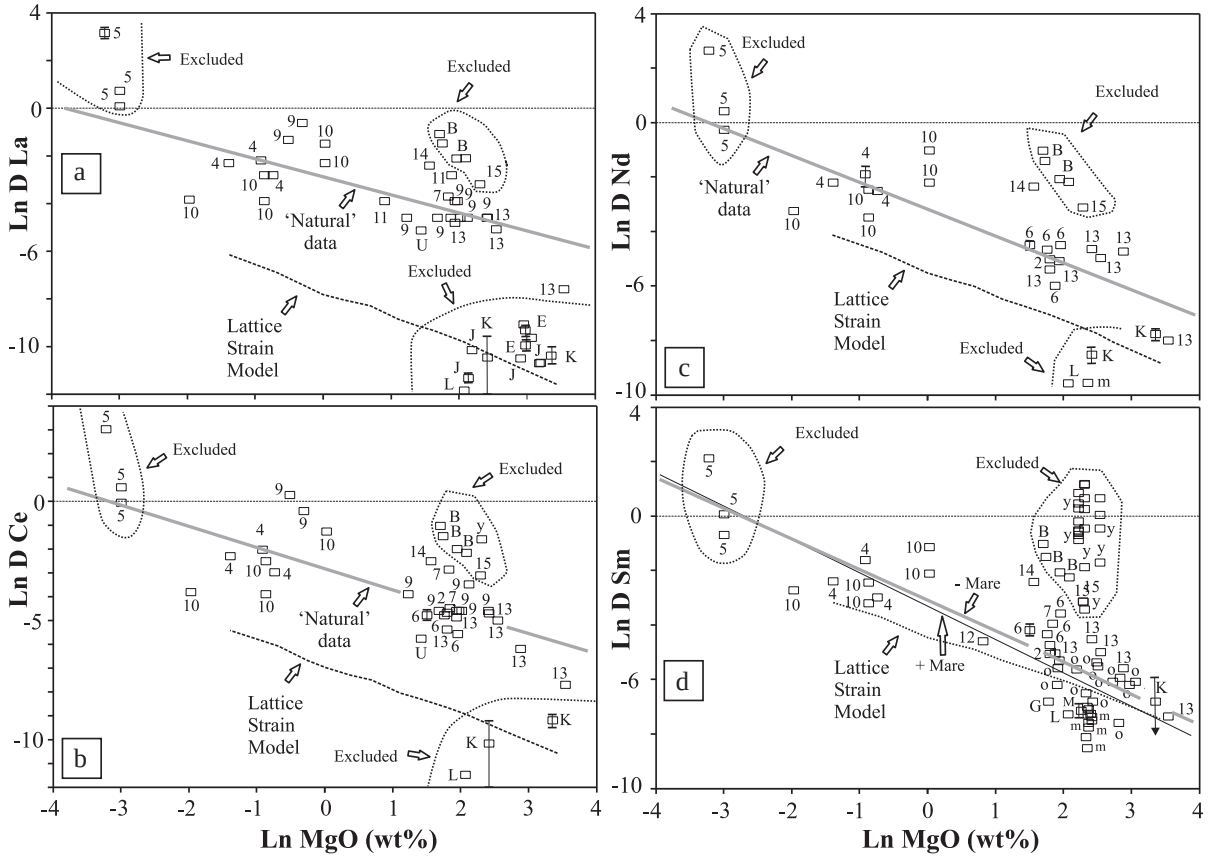

Fig. 9. (a) Ln *D* La, (b) Ln *D* Ce, (c) Ln *D* Nd, and d) Ln *D* Sm vs. Ln MgO (wt.%). Predictions of the Lattice Strain Model (see below) are generally lower than the regression results. Thick grey lines are regressions or averages of mostly 'natural' data (Table 2). Ln *D* regressions that exclude and include Lunar Mare data (−Mare and +Mare, respectively) are shown.

as two segments with a cusp at MgO#=8.35 (Table 2). The mafic trend applies to data with SiO_2<60 wt.%; while the felsic trend was calculated for data with MgO#<10. One potential cause of scatter in MgO# is the decoupling of melt FeO and temperature (e.g. Sugawara, 2000, his Fig. 2), which generates variability in the FeO/MgO ratios of the melt and the minerals crystallizing from it at a given temperature and melt MgO content.

2.3.2. SiO_2

For mafic and ultramafic melts, values of Ln *D* Ti show extensive scatter below 55 wt.% SiO_2 (2 Ln units, Fig. 4b), with a better defined increase in *D* Ti for melt SiO_2>55 wt.%. The data were regressed as two segments with a cusp at 55 wt.% SiO_2 (Table 2). The 'X' symbols are discrepant data (crosses in Figs. 2 and 3) that were included in the regression against SiO_2. The extensive scatter of *D* Ti values in the 44–55% SiO_2-range may reflect the fact that melts perched on the olivine–plagioclase–clinopyroxene cotectic can evolve considerably in terms of temperature and MgO content with little corresponding change in SiO_2 content.

2.3.3. MgO

Values of *D* Ti for melts of ultramafic to intermediate composition define a diffuse trend of increase as MgO decreases, with low-MgO felsic melts showing a steeper trend of *D* Ti increase (Fig. 4c). The data were regressed as distinct mafic and felsic segments with a cusp at 0.493 wt.% MgO. The Ln *D* Ti vs. MgO regression for mafic melts showed marginally better statistics, with correlation coeffi-

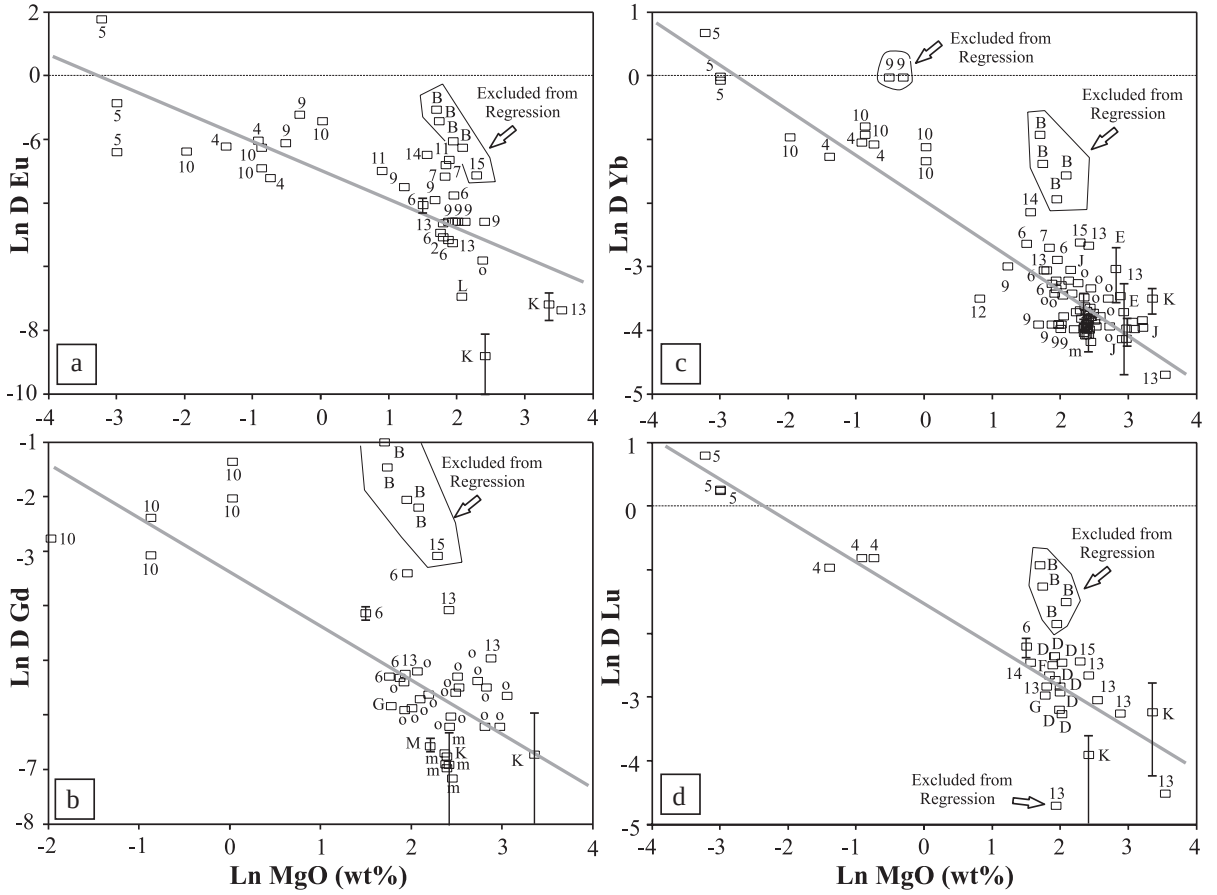

Fig. 10. (a) Ln *D* Eu, (b) Ln *D* Gd, (c) Ln *D* Yb, and (d) Ln *D* Lu vs. Ln MgO (wt.%). Thick grey lines are regressions or averages (Table 2).

cients of the same order as the regression against temperature (Table 2).

3. Parameterization of $^{olivine/liquid}D$ for trace elements

3.1. Choice of input variable for the parameterization

Regressions of *D* Ti (and other elements) against temperature show reasonable trends (e.g. Fig. 2), but temperature is difficult to estimate in natural situations, and there are few felsic data with which to constrain the low-temperature end of the spectrum. Trends of *D* Ti vs. pressure, water content, and olivine forsterite content are unconvincing (Fig. 3a–c), and the Fo-content is sensitive to subsolidus effects (see above, Section 2.2). Although valid in some contexts, use of complex melt functions was not considered for the reasons explained previously (Section 1.3). Among the simple melt compositional parameters examined, the correlations against melt MgO# were generally quite diffuse (Fig. 4a), although tighter trends were observed for some other elements (e.g. *D* Sc, Fig. 5b). Plots against melt SiO_2 are scattered for melts of ultramafic to intermediate composition (Figs. 4b and 5a), but yield reasonable regressions for felsic melts. For most of the partitioning data examined, melt MgO content provided the best correlations (Figs. 4c and 5c,d). Consequently, melt MgO content was chosen as the variable against which to parameterize *D* variations for all trace elements, in part to minimize errors on calculated *D*/*D* ratios. Using melt MgO content also has many advantages for the

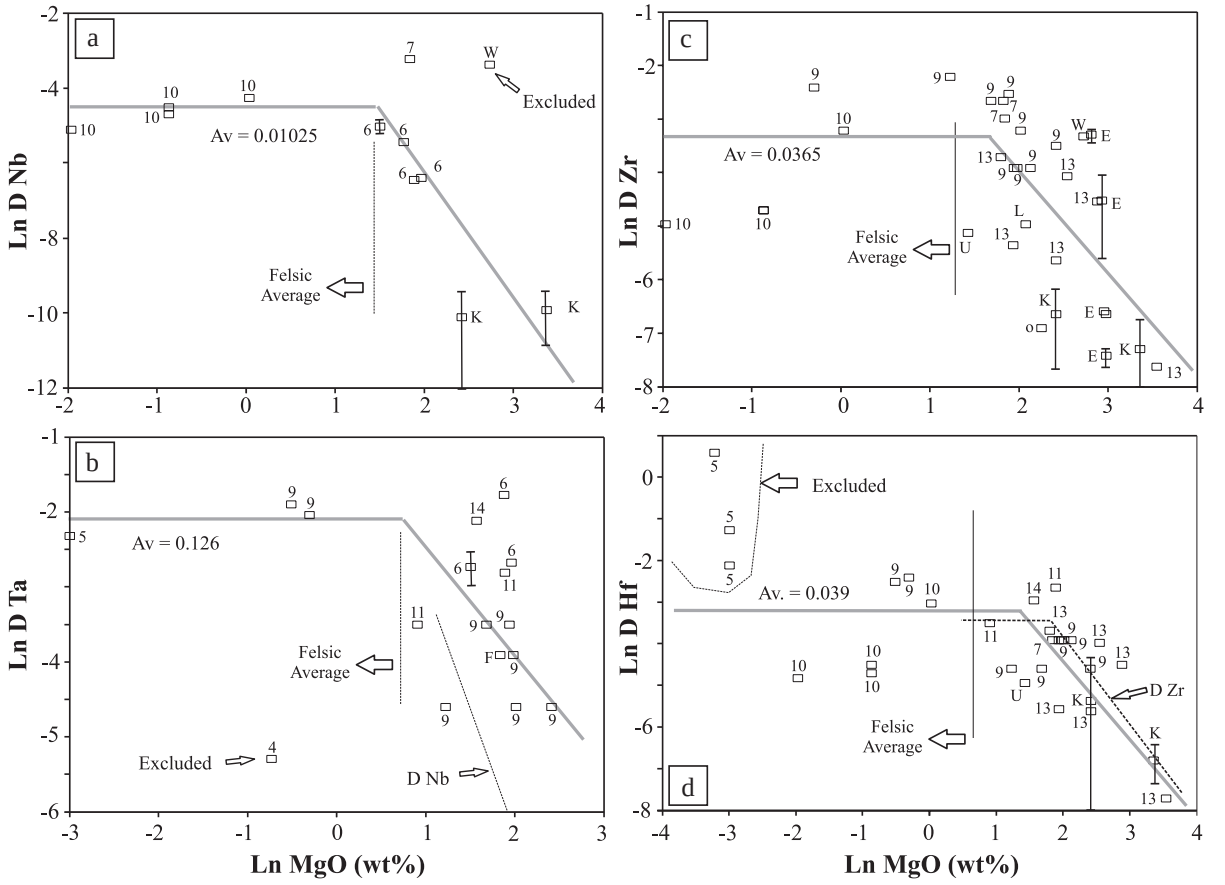

Fig. 11. (a) Ln *D* Nb, (b) Ln *D* Ta, (c) Ln *D* Zr, and (d) Ln *D* Hf vs. Ln MgO (wt.%). Thick grey lines are regressions or averages (Table 2). In 'b' the *D* Ta line was fit by eye, and the *D* Nb regression is shown for comparison.

geochemical modeler, inasmuch as MgO is closely linked to temperature (Sugawara, 2000, and Fig. 1a; Table 2), and can be calculated from mineral analyses (e.g. Maclennan et al., 2003).

3.2. Metals (Sc, Cr, Al, Zn, Co, Ru, Rh, Re, Os, Ni, V)

3.2.1. D Sc

Values of Ln *D* Sc increase systematically for melt SiO_2>60 wt.% (Fig. 5a), but exhibit considerable dispersion for SiO_2 between 40% and 55%. The plots against liquid MgO# (Fig. 5b) or Fo-content (not shown) show much scatter. The plot against the MgO-content of the liquid shows a good correlation (Fig. 5c,d), and arguably, scatters least. Representative error estimates from the original papers are shown, and most data appear to be within error of the regression. Two *D* Sc determinations from Kennedy et al. (1993, 'K') and a Datum from Nielsen et al. (1992, 'G') have *D* Sc that plot much higher than do other determinations at a similar MgO contents (Fig. 5bc). The synthetic melts ('K') have unusually high SiO_2 (Fig. 5a), high FeO (9–17 wt.%), and no alkalis. Which of these features (if any) are responsible for the high *D* Sc values of these two runs is not clear. Because of these uncertainties, these three discrepant points were excluded from the regressions.

3.2.2. D Cr

For MgO contents >10%, the *D* Cr data are very coherent (Fig. 6b), and the vast majority of *D* Cr determinations can be regressed together (Fig. 6a). At lower MgO contents, the data show

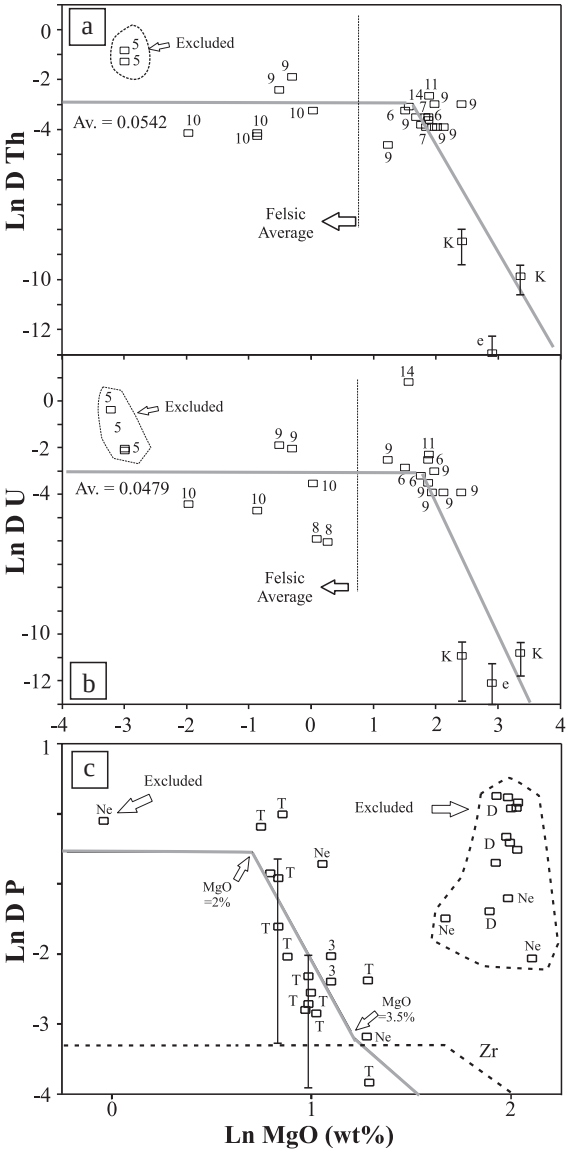

Fig. 12. (a) Ln *D* Th, (b) Ln *D* U, (c) Ln *D* P vs. Ln MgO (wt.%). Thick grey lines are regressions or averages (Table 2). Values of the *D* Nb and *D* Zr regressions are shown in 'c' for comparison. Values of *D* P are assumed to plateau out for compositions more felsic than MgO=2 wt.%. For values of MgO>3.5%, the Ln *D*P vs. Ln MgO line was assumed to have a slope similar to that of the *D* Zr regression.

considerable scatter, presumably reflecting the combined effects of variations in oxygen fugacity, temperature, melt composition, Cr speciation in the melt and crystal-field effects (Schreiber and Haskin, 1976; Suzuki and Akaogi, 1995; Hanson and Jones, 1998; Colson et al., 2000). In addition, most low-MgO melts are poor in Cr, suggesting that *D* Cr values for low MgO melts may be less accurate and precise than those from Cr-rich, high-MgO experiments.

Strongly reduced lunar magmas are expected to have a large proportion of Cr^{2+} in the melt, while more oxidized terrestrial magmas have little or none (Schreiber and Haskin, 1976).Values of *D* Cr^{2+} calculated from the expression in Hanson and Jones (1998, *D* $Cr^{2+}=0.66\ (10{,}000/T\ \mathrm{K})-4.48$), applicable to terrestrial magmas, are zero at temperatures >1473.2 K, and increase slowly until about 1200 K, after which values rise more quickly (Fig. 6b). Values of *D* Cr^{2+} are typically very much smaller than *D* Cr^{total} and should have little impact on *D* Cr^{total} for MgO>5 wt.%. Hanson and Jones (1998) also proposed that *D* $Cr^{3+}=-0.39(NBO/T)+1.29$, where NBO/T is the ratio of non-bridging oxygens to tetrahedrally coordinated cations (Mysen, 1983). Not all of the data needed to calculate NBO/T have been compiled here, but the ratio of SiO_2/MgO wt.% (network former/modifier) may serve as a proxy. Plots of *D* Cr^{2+} vs. SiO_2/MgO wt.% appear to define a straight line (Fig. 6c) which was regressed (Table 2). Subtracting the value of *D* Cr^{2+} calculated as suggested by Hanson and Jones (1998) from the measured value of *D* Cr^{total} yields a value for *D* Cr^{3+}, which seems well clustered when plotted against SiO_2/MgO wt.% (Fig. 6c), except for high-SiO_2/low MgO data, which scatter widely and which were not included in the regression (only data for MgO>2.5 wt.% were included). Both approaches yield comparable results (Fig. 6b) for mafic melts, and so the simpler *D* Cr^{total} regression is preferred.

3.2.3. D Al

D Al data show a clear trend of increase with increasing pressure for mafic–ultramafic melts (Fig. 7a; Table 2). Low-pressure (<0.5 GPa) data for *D* Al show very scattered trends against melt MgO content (not shown), and two averages (for MgO>3% and MgO<3%) were calculated (Table 2).

3.2.4. D Zn

Most *D* Zn data are from Kohn and Schofield (1994) and yield very good correlations (Fig. 7b). *D*

Table 2
Regression results

	Range	*Y* intercept	Standard error *Y*	R^2	*N*	Slope *X*	Standard error *X*
vs. temperature in K							
D Ti	Mafics	0.064768	0.012245	0.0797	354	−2.373e−05	4.2969e−06
Ln *D* Ti	Mafics	−2.25688	0.449943	0.0880	354	−0.0009202	0.0001579
vs. pressure in GPa							
D Ti	SiO_2<60%	0.031200	0.012548	0.0330	354	−0.002472	0.000713
D Al	*P*>0.8 GPa	0	0.003200	0.8187	299	0.0051600	8.350e−05
vs. wt.% H_2O in melt							
D Ti		0.031795	0.011777	0.0008	97	0.000130	0.000494
vs. 100MgO/MgO+FeO^{total} wt.% in melt							
D Ti	SiO_2<60%	0.0373594	0.012286	0.0587	366	−0.0001927	4.0443e−05
D Ti	MgO#<8.35	0.3199849	0.109968	0.5402	10	−0.034200	0.011156
vs. SiO_2 wt.% in melt							
Ln *D* Ti	SiO_2<57.0967%	−4.956987	0.478451	0.0339	298	0.026060	0.008092
Ln *D* Ti	SiO_2>57.0967%	−9.718522	0.447954	0.5787	81	0.109454	0.010506
Ln *D* Sc	All	−6.603421	0.486269	0.7032	70	0.105354	0.008299
vs. MgO wt.% in melt							
T °K	MgO<2%	1097.2721	96.32468	0.4217	17	128.5956	38.88502
T °K	MgO 2–14%	1269.8519	70.00587	0.6203	635	25.78361	0.801853
T °K	MgO>14%	1217.6602	82.36312	0.5817	203	27.98546	1.673959
D Ti	MgO>0.493%	0.0378058	0.019702	0.0477	366	−0.000940	0.000220
D Ti	MgO<0.493%	0.287680	0.134368	0.3821	8	−0.518924	0.269424
Ln *D* Ti	MgO>0.493%	−3.341999	0.457732	0.1108	366	−0.034417	0.005111
D Re	MgO 6–16%	0.434801	0.038140	0.9181	7	−0.025012	0.003340
D Os	MgO 6–16%	0.076084	0.008095	0.8964	7	−0.004664	0.000709
vs. Ln MgO wt.% in melt							
Ln *D* Cs,K,Rb	MgO>1.11%	0.052277				−3.048573	
Ln *D* Ba	MgO>1.125%	1.220691	2.492188	0.5937	20	−4.078261	0.795201
Ln *D* Sr	MgO>1.04%	−0.103745	2.040069	0.4795	24	−2.701496	0.600062
Ln *D* Pb	MgO>0.45%	−0.960117	1.286470	0.7468	5	−2.365962	0.795375
Ln *D* Th	MgO>4.9037%	3.805739	1.857101	0.5826	18	−4.221746	0.893387
Ln *D* U	MgO>5.91%	7.079996	2.155782	0.7038	14	−5.674872	1.062760
Ln *D* Nb	MgO>4.47%	0.281997	1.637831	0.6511	7	−3.295911	1.079028
Ln *D* Ta	MgO>4.4%	0				−1.5	
Ln *D* P	MgO>3.5%	−0.2				−2.5	
Ln *D* P	2<MgO<3.5%	2.922448	0.705766	0.5922	15	−4.993652	1.149384
Ln *D* Zr	MgO>5.2%	−0.254395	1.291158	0.4313	27	−1.879372	0.431619
Ln *D* Hf	MgO>1.38%	−2.985779	1.002827	0.6808	23	−0.760857	0.113676
Ln *D* La	Natural	−2.896755	1.067633	0.5152	26	−0.749805	0.148474
Ln *D* Ce	Natural	−2.855783	1.204564	0.5359	29	−0.906973	0.162432
Ln *D* Nd	Natural	−3.166716	1.461593	0.5434	20	−0.980556	0.211838
Ln *D* Sm	−Mare	−3.261860	1.152858	0.6395	44	−1.143695	0.132508
Ln *D* Sm	+Mare	−3.378820	1.224925	0.6034	53	−2.334665	0.138915
Ln *D* Eu	All	−2.966757	1.241378	0.6342	37	−0.905163	0.116190
Ln *D* Gd	All	−3.407878	0.917655	0.6146	37	−0.977639	0.130870
Ln *D* Tb	All	−2.697347	0.942221	0.7674	30	−0.865027	0.090000
Ln *D* Dy	All	−2.641279	0.770337	0.8724	21	−0.904799	0.079403
Ln *D* Y	All	−2.673573	1.101424	0.4249	19	−0.661902	0.186190

(continued on next page)

Table 2 (*continued*)

	Range	*Y* intercept	Standard error *Y*	R^2	*N*	Slope *X*	Standard error *X*
Ln *D* Ho	All	−2.316611	0.843870	0.6993	16	−0.83043	0.145549
Ln *D* Er	All	−2.229420	0.710297	0.7006	19	−0.697091	0.110519
Ln *D* Yb	All	−1.952636	0.418793	0.8561	76	−0.713368	0.033992
Ln *D* Lu	All	−1.523311	0.360950	0.9261	26	−0.643206	0.037087
Ln *D* Cr	All	1.346400	0.504824	0.3650	421	−0.654416	0.042170
Ln *D* Co	MgO>0.5%	3.238143	0.308432	0.8017	22	−0.899993	0.100081
Ln *D* Zn	MgO>1%	1.695972	0.093334	0.9766	28	−0.674038	0.020442
Ln *D* Sc		−0.207763	0.255686	0.9196	67	−0.614241	0.022531
Ln *D* Na		−4.507033	0.850363	0.0637	84	−0.179334	0.075907
vs. SiO_2/MgO wt.% in melt for MgO>2.5%							
D Cr^{2+}	*T*<1473 K	−0.086472	0.105407	0.7225	66	0.027712	0.002147
D Cr^{3+}	MgO>4%	0	0.704659	0.0543	392	0.187641	0.007579

		Averages	*N* Data	Standard deviation	Source
D Cs–K–Rb	MgO<1.11%	0.0353	17	0.0334	
D Ba	MgO<1.125%	0.036	6	0.0343	
D Pb	MgO<0.45%	0.132	4	0.0449	
D Sr	MgO<1.04%	0.054	3	0.0143	
D Th	MgO<4.904%	0.0542	6	0.0504	
D U	MgO<5.91%	0.0479	7	0.0591	
D Nb	MgO<4.4%	0.01025	4	0.00303	
D Ta	MgO<3.79%	0.126	3	0.0214	
D Zr	MgO<5.2%	0.0365	4	0.0336	
D Hf	MgO<1.38%	0.0394	7	0.0318	
D P	MgO<2%	0.5834	assumed		
D Co	MgO<0.5%	16.63	8	7.27	
D Al	MgO>3%, *P*<0.8 GPa	0.00889	211	0.01177	
D Al	MgO<3%, *P*<0.8 GPa	0.01184	31	0.01430	
D Zn	MgO<1%	10.73	3	0.29	(5)
D Cu		0.11	2	–	(1,u)
D Ag		0.38	1	–	(W)
D Au		0.1258	1	–	(I)
D Li		0.198	2	–	(u,U)
D Be		0.2475	2	0.2125	(6)
D Mo		0.1034	5	0.4000	(10,6)
D Sn		0.119	1	–	(10)
D Sb		0.1938	8	0.1668	(11,9)
D Mo		0.1034	5	0.0400	(6,10)
D Sb	Mafic	0.0925	4	0.0334	(9)
D Sb	Felsic	0.44	2	–	(9)
D Ga		0.1026	4	0.1243	(E)
D Cd		0.082	1	–	(u)
D Pd	(carbonatite)	2.3	1	–	(W)
D Pd	(silicate melt)	0.02604	12	0.03181	(b,I,17, exclude 1 value from Ca)
D Pt		0.05136	2	0.01340	(17)
D Ru		0.66575	7	0.37070	(b,I,17,Ca: exclude 1 value from b)
D Rh		2.69581	9	1.41070	(b,Ca)
D Re	MgO<8 wt.%	0.27048	2	0.07292	(16)
D Re	MgO>8 wt.%	0.03816	8	0.01856	(I,16)
D Os	MgO<20 wt.%	0.01448	7	0.02126	(16)
D Os	MgO>20 wt.%	0.53437	2	0.10393	(17)
D Ir		0.42619	2	0.07381	(17)

Zn measurements from some older studies are discrepant and were not included in the regression. The scanty felsic data were averaged (Table 2).

3.2.5. D Co

Data for *D* Co yield a good regression (Fig. 7c) for mafic melt compositions. A single datum from Wörner et al. (1983, '14') was excluded, since the melt MgO content for this datum is poorly constrained. A separate average value was calculated for low MgO melts (Table 2).

3.2.6. Pt, Pd, Ru, Rh, Re, Os, Ir

Data on Platinum Group Elements are sparse, and few systematic trends were seen (Table 2). Data on *D* Pd from a carbonatite (*D* Pd=2.3, Sweeney et al., 1995) is much higher than data from silicate melts (av.=0.026). A single, very high value of *D* Ru=2.2 from Brenan et al. (2003) was excluded from the average. Data on *D* Re appear to define two groups, with two data from melts with MgO<8 wt.% being much higher than data from melts with MgO>8 wt.%. Data for *D* Os shows the opposite pattern, with two data from melts with MgO>20 wt.% from Puchtel et al. (2004) being much higher than data from Burton et al. (2002) from melts with lower MgO contents.

3.2.7. D Ni, D V

Many papers deal with how *D* Ni varies with melt composition, the more recent of which (Kinzler et al., 1990; Li et al., 2003, see Table 2) incorporate the effects of the melt FeO/MgO ratio and olivine Fo-content, yielding prediction errors of ca. 13%. Canil and Fedortchouk (2001) have recently parameterized how *D* V varies with oxygen fugacity (Table 2).

3.3. Large ion lithophile elements (LILE): (Cs, Rb, K, Na, Ba, Sr, Pb)

Data for *D* Cs, *D* Rb and *D* K are sparse, scattered, and apart from some imprecise *D* K measurements calculated from the data in phase equilibrium studies, are unavailable for high-MgO systems (Fig. 8a). Data for *D* Sr, *D* Ba and *D* Pb also show considerable scatter, but do include values from high-MgO melts (Fig. 8a,b). A further complication is the tendency for these partitioning data to form three non-colinear clusters. Cluster 1 comprises very low *D* values from high-MgO melts (Kennedy et al., 1993 'K'; Beattie, 1993 'e' and 1994 'J'; Purton et al., 2000 'u'). Cluster 2 is constituted mostly of natural data from basaltic to intermediate melts, and have higher *D* values than the 1st cluster. Cluster 3 comprises data from low-MgO melts, with *D* values only slightly higher than the 2nd cluster.

Why are there three clusters? The high-MgO, low-*D* cluster is principally constituted by data from Beattie (1993, 1994) and Kennedy et al. (1993). The error estimates (e.g. see *D* Sr, Fig. 8b) would imply that the extremely low *D* values are not analytical artefacts. The other clusters are constituted by data from many different studies, which would seem to preclude a systematic analytical or laboratory errors. Since the 2nd (basaltic) cluster is constituted principally of natural data, the high *D* values of

Notes to Table 2:

$^{olivine/liquid}D$ parameterization. Gives values of the slope '*X*' and intercept '*Y*' allowing *D* values to be calculated from the melt MgO (wt.%) content, and estimates of the errors on the regressions and the fit (R^2). Average values are given where data were inadequate to allow regression, as well as the applicable MgO range. Some of the data from Mahood and Hildreth (1983) were excluded from the felsic averages for Th, U, Hf and LILE because of probable trace mineral contamination (Michael, 1988). Equations for *D* Ni are from Arndt (1977), Hart and Davis (1978), Kinzler et al. (1990), and Li et al. (2001). The *D* V equation is from Canil and Fedortchouk (2001). Equations for *D* Cr are from Hanson and Jones (1998).

Expressions from the literature

D Ni=115/(MgO wt.%)−2.1 (Arndt, 1977).

D Ni=124/(MgO wt.%)−0.9 (Hart and Davis, 1978).

Ln (*D* Ni wt/Fo mole fraction)=0.355−1.263 Ln MgO (mol% in liquid) (Kinzler et al., 1990).

Ln *D* Ni=5.67−1.38 Ln MgO (wt.%)−0.25 (FeO/MgO) (Li et al., 2001).

Log *D* V=−0.23ΔNNO−1.46 (Canil and Fedortchouk, 2001).

D Cr^{2+} =0.66 (10,000/*T* °K)−4.48) (Hanson and Jones, 1998).

D Cr^{3+} =−0.39 (NBO/T)+1.29 (Hanson and Jones, 1998; Mysen, 1983).

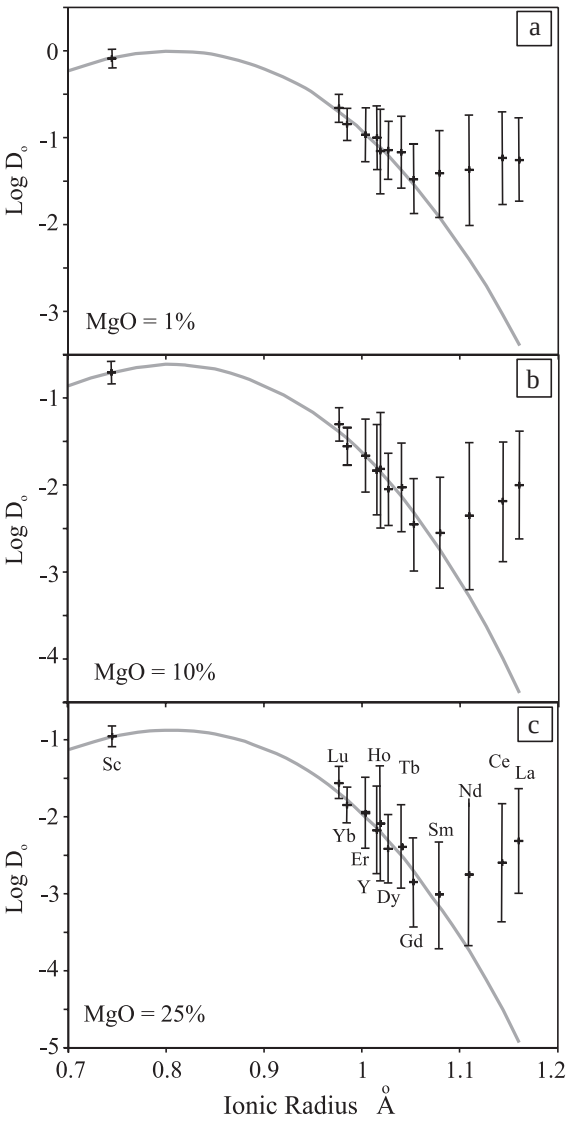

Fig. 13. (a) Comparison of predicted values of Log D from the Lattice Strain Model (Eq. (1), grey curve), with regressions of Table 2 (crosses) for three representative liquid MgO contents. Values of E_M^{3+}, r_0, and D_0 were allowed to vary until a satisfactory visual fit was obtained. Only D's for the middle and heavy REE, Y and Sc were used to adjust the fit. Temperature was calculated using equations in Table 2 (Fig. 1a). Note that values of D La, D Ce and D Nd calculated with the Lattice Strain Model are significantly below most experimental and natural values, which form a plateau, interpreted to be due to kinetic effects (Kennedy et al., 1993). Note that this plateau effect appears to become more pronounced as the MgO content decreases. Ionic radii are from Shannon (1976).

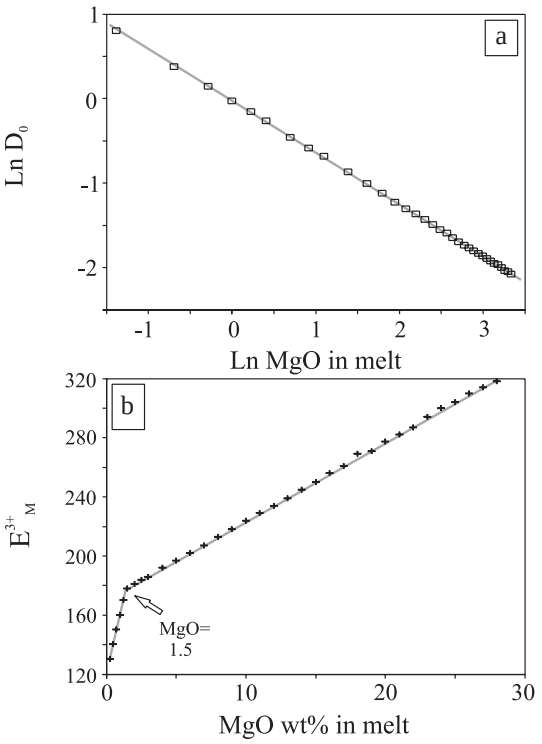

Fig. 14. (a) Ln D_0 (strain-compensated partition coefficient) vs. Ln MgO wt.% in melt, and (b) E_M^{3+} (Young's Modulus) vs. MgO wt.% in melt. Datapoints were derived by fits like those of Fig. 13. Thick grey lines are regressions from Table 3.

the 2nd cluster may reflect the presence of melt or solid inclusions in the analyzed material (cf. Kennedy et al., 1993). The lack of continued increase in D values as MgO decreases (cluster 3) might be attributed to a change in the crystal chemistry of Fe-rich olivines; but cell parameters increase linearly from forsterite to fayalite (Brown, 1982), which suggests that this cannot be the explanation.

Until these problems are resolved, any parameterization of D for the LILE will remain uncertain. Nevertheless, as a 1st approximation, data from ultramafic and mafic melt compositions (clusters 1 and 2, Fig. 8b) for D Sr, D Ba and D Pb were regressed for each of these elements (Table 2). Data from felsic melt compositions were averaged for each element (Table 2; Fig. 8a). Because of their sparsity, felsic data for D K, D Rb and D Cs were averaged together (Fig. 8a). Two D K determinations from

Table 3
Results of regressions for D_0 and E_M^{3+}

	Y intercept	Standard error Y	R^2	#	Slope X	Standard error X
vs. Ln MgO						
Ln D_0 All	−0.02713243	0.00891947	0.999	34	−0.6126633	0.0011471
vs. MgO						
E_M^{3+} MgO>1.5%	170.1960	0.809903	0.999	29	5.346736	0.018326
E_M^{3+} MgO<1.5%	120.6667	0.690066	0.999	6	38.85714	0.659829

Parameterization for E_M^{3+} and D_0 vs. MgO or Ln MgO (respectively), which feed into the Brice (1975) equation (Eq. (1)), allowing calculation of D REE, D Y, and D Sc from MgO in the liquid. Values of r_0 were assumed constant at 0.807 Å.

Scaillet and MacDonald (2001) plot offscale, but were included in the averages. D K data for high-MgO melts from the phase equilibrium study of Wasylenki et al. (2003) plot anomalously and were not used. Since there are no reliable high-MgO partitioning data for K, Rb and Cs, I assumed that they would be in the same range as Sr, Ba and Pb, and computed an average regression from the D Sr–Ba–Pb data (Fig. 8a).

Scattered D Na data increase as MgO decreases (Fig. 8c), but no other obvious trends were detected against any other variable.

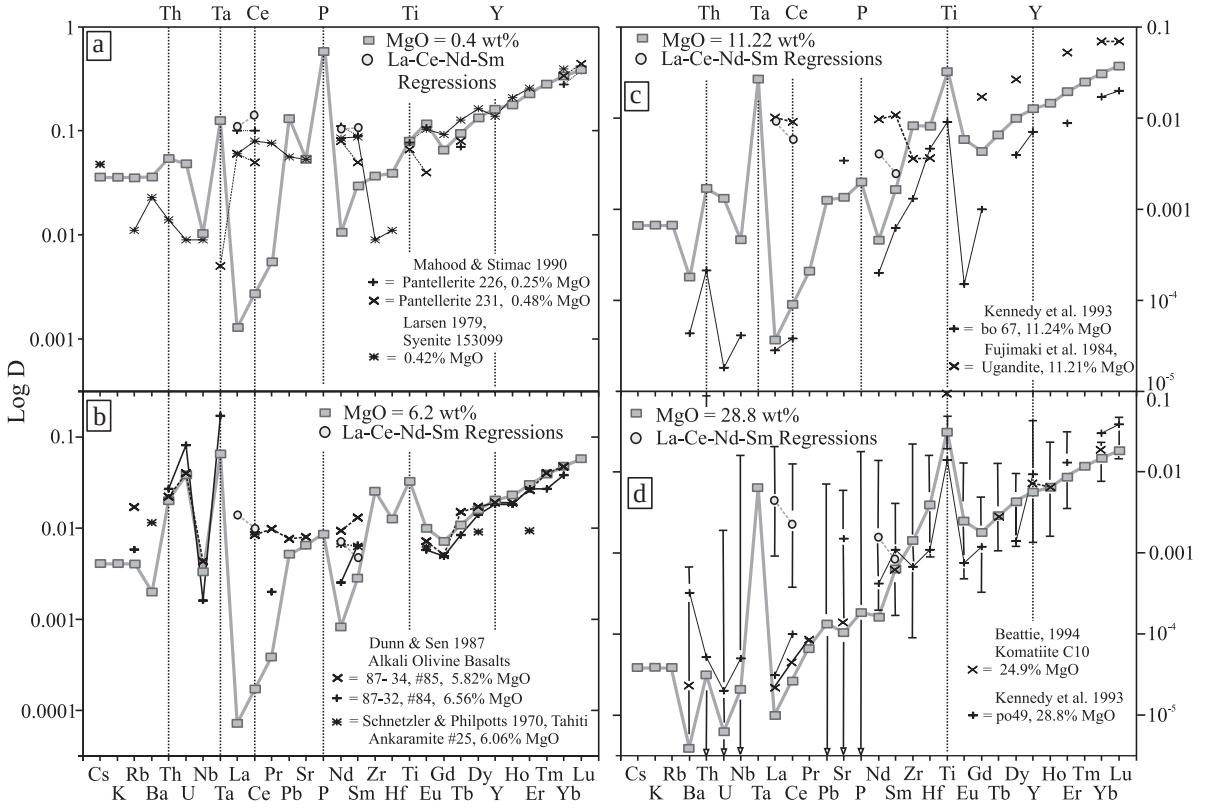

Fig. 15. Comparison of typical experimental partitioning data with results (grey boxes) of the composite parameterization (Tables 2 and 3). The circles show results of the D La, D Ce, D Nd and D Sm regressions (Table 2), to illustrate the 'plateau' effect for these data. Error estimates for the regressions of Table 2 are shown in 'd'.

3.4. Highly charged cations (rare earths, Y, Nb, Ta, U, Th, Zr, Hf, P)

3.4.1. Rare earths, Y

Variations of *D* REE are constrained by reasonably large datasets (Figs. 9 and 10) that extend from high- to low-MgO melt compositions. The middle and heavy REE (Sm, Gd, Tb, Dy, Ho, Er, Tm, Yb and Lu) display coherent behaviour, with all except the oldest data forming a single trend that was regressed (Fig. 10; Table 2). In contrast, partitioning data for the Light REE (LREE) La, Ce, Nd, Sm (Fig. 9) and Eu (Fig. 10) display a complex distribution similar to the one observed for the LILE (Fig. 8). The LREE partitioning data from Kennedy et al. (1993), Beattie (1994), Canil and Fedortchouk (2001) and McKay (1986) tend to plot below the main trend of the data, while some older data (Shimizu et al., 1982, 'B' and '15'; Mysen, 1978, 'y') plot above it. As a first approximation, I calculated regressions for the mafic to felsic spectrum, ignoring the low-*D* high-MgO data cluster. The data that were regressed are almost entirely 'natural' data and provide a benchmark against which to compare results of the Lattice Strain Model (see below). A few natural data with uncertain MgO contents (LeMarchand et al., 1987, '9') were excluded from the regressions, as were the data of Mahood and Hildreth (1983, '5') which are probably contaminated with LREE-enriched trace phases (Michael, 1988).

3.4.2. D Nb, D Ta, D Zr, D Hf, D Th, D U

There are few *D* Nb and *D* Ta data, and there is considerable scatter, making regressions problematic (Fig. 11a,b). For *D* Nb, ultramafic–mafic data were regressed, while felsic data were averaged (Fig. 11a; Table 2). A single datum from Sweeney et al. (1995, 'W') was excluded from the regression. This datum is from a carbonatitic melt, and as there was no equivalent *D* Ta determination, I excluded the *D* Nb value to avoid creating a bias when comparing *D* Nb to *D* Ta. The *D* Ta data scatter considerably and did not yield a reasonable regression, and so a line was passed through the main cloud of *D* Ta data to join the felsic *D* Ta average. Note that all existing *D* Ta data is 'natural'. More experimental *D* Ta and *D* Nb data are badly needed.

For *D* Zr, *D* Hf, *D* Th, *D* U, partitioning data from ultramafic–mafic melts were regressed, while *D* data from felsic melts were averaged (Figs. 11c,d and 12a,b; Table 2). *D* Hf data from Mahood and Hildreth (1983) were not included in the average because they appear to be anomalously high, and may have been perturbed by trace mineral inclusions (Michael, 1988).

3.4.3. D P

Most of the D P data define a reasonable correlation (Fig. 12c), but the range of MgO contents controlling the regression is narrow (2.1–3.6 wt.% MgO), and the steep slope is quite different from that of other highly charged cations. Use of such a steep slope would generate prominent negative *D* P anomalies in the *D* profiles for high-MgO melt compositions, and large positive anomalies for felsic melt compositions. To avoid these modeling artefacts, I assumed that *D* P will behave similarly to other HFSC and assigned a slope similar to the slope of the *D* Zr regression for MgO contents >3.5%. Since high P_2O_5 is not reported from Fe-rich olivines, I assumed that *D* P plateaus out for MgO contents <2 wt.%. The data of Dunn (1987, 'D') appear to be anomalously high and were not included in the regression. Data from Nekvasil et al. (2004) also show considerable scatter, and were not included in the regression.

4. Comparison with the Lattice Strain Model (LSM)

It has long been known that trace element partition coefficients show a maximum value centered at the ionic radius of the host site (Onuma et al., 1968). This has been formalized by Brice (1975) and Blundy and Wood (1994a,b) and is commonly referred to as the Lattice Strain Model (LSM), or as the Brice equation. The LSM posits a parabolic distribution of Log *D* values around the ionic radius of the host site 'r_0', which gives the position of the curve apex on the ionic radius axis (e.g. Fig. 13). The Blundy and Wood (1994a,b) expression is:

$$D_i = D_0 \exp(-4\pi E N_A((r_0/2)(r_i - r_0)^2 + 1/3(r_i - r_0)^3)/RT) \quad (1)$$

where D_0 is the strain compensated partition coefficient, giving the *D* value of the curve's apex; r_0 is the ionic radius of the cation of interest (taken from

Shannon, 1976); E is the Young's Modulus of the host site, which affects the shape of the model curve; N_A is Avogadro's number; R is the gas constant and T is temperature in degrees Kelvin, here calculated from the temperature–MgO regressions of Table 2 (Fig. 1a).

Values of D_0, E and r_0 are commonly determined by fitting the LSM to sets of experimental partitioning data (e.g., see Wood and Blundy, 1997; Hill et al., 2000). Trace element D values for the rare earths, Y and Sc obtained from the regressions of Table 2 were compared visually to results of the LSM for many different MgO contents (Fig. 13). The position and shape of the model curves are extremely sensitive to changes in D_0, E and r_0, which were allowed to vary so as to pass the model curves through the main Sc–HREE–MREE distribution (HREE and MREE are heavy and middle rare earth elements, respectively). As suggested by Kennedy et al. (1993), D Sc is near the apex of the model curves and a constant value of r_0=0.807 Å was found to yield reasonable fits for all models. Derived values of E_M^{3+} yield tight linear correlations with MgO in the liquid, with an inflection at MgO=1.5 wt.% (Fig. 14a). The decrease in E_M^{3+} implies that the D profile will 'flatten' as the melt evolves. Trivalent cations such as Cr, Sc and the REE appear to enter olivine as a coupled substitution with Al (Schreiber and Haskin, 1976; Beattie, 1994), partitioning into two non-equivalent octahedral sites (Brown, 1982). Consequently, the values of E_M^{3+} derived here represent composites for the two olivine M sites. Ln D_0 is also very well correlated with Ln MgO (Table 3; Fig. 14b), and shows a steady increase. These excellent correlations (Fig. 14) suggest that D_0 and E_M^{3+} are adequately parameterized in this manner, and that the LSM can be used in conjunctions with the equations in Table 3 to calculate equilibrium values of D for these elements at any MgO content.

Although the D values for middle- and heavy-REE, Y and Sc plot along the trends predicted by the LSM, the D for the LREE (Nd–Ce–La) form a plateau (Fig. 13), with the plateau effect extending to D Sm as melts become cooler and more evolved (Fig. 13a). In contrast, modern high-quality experimental data plot along the trend expected from the Lattice Strain Model (Figs. 4 and 15). Kennedy et al. (1993) concluded that high cooling rates (>500 °C/h) prevent the establishment of complete equilibrium, with the trace element enrichment (plateau effect) being accounted for by the incorporation of small amounts (<1%) of trapped melt (cf. Beattie, 1994).

5. Discussion

Results of the LSM parameterization (Table 3) for calculation of D REE–Y–Sc are combined with the regressions for other elements (Table 2) to produce multi-element D plots for different MgO contents (0.4, 6.2, 11.22, 28.8 wt.% MgO, Fig. 15). Fig. 15d compares the model D profile (boxes) at 28.8% MgO to experiment po49 from Kennedy et al. (1993) and C10 from Beattie (1994). Overall, the data from Kennedy et al. (1993) and Beattie (1994) are very similar to the model profile. Note the prominent positive D Ti and D Ta anomalies in the model, and the absence of a D Nb anomaly. If the model D values are taken at face value, the implication is that high-MgO komatiitic melts equilibrating with dunitic residua should develop small negative Ti–Ta anomalies, and might fractionate Nb from Ta, and Zr from Hf.

With further cooling and melt evolution (Fig. 15c), the overall model D abundances increase progressively (cf. Fig. 14a), and the profile shape flattens (cf. Fig. 14b). The model profile shape for primitive basalts (11.22 wt.% MgO) is broadly similar to those of available experimental D profiles (Fig. 14c). The slowly cooled experiments (bo67) of Kennedy et al. (1993) conform to the model D profile predicted by the LSM (boxes), while the natural data of Fujimaki et al. (1984) more closely resemble the regressions of Table 2 (circles), perhaps indicating a kinetic limit on partitioning of the LREE, as proposed by Kennedy et al. (1993). Note also that the positive D Zr, D Hf, and D Ti anomalies have increased in size, the apparent D Ta anomaly remains prominent, and that the D Zr/D Hf ratio has increased (Fig. 15c).

For basaltic melt compositions, the model D profile shape closely resembles the existing experimental data (6.2% MgO, Fig. 15b), except for the D LREE data, which show the plateau effect discussed above. Positive D U and D Th anomalies have appeared, the D Ta anomaly remains prominent, while the D Ti anomaly has decreased in size (Fig. 15b). The positive D Zr and D Hf anomalies have increased in size and D Zr/D Hf has increased. However, the scatter for D Zr and D Hf is extensive

(Fig. 11d), and the changes in model D Zr/D Hf are probably not significant. For more evolved melts, the absolute values of D continue to increase for most elements (Figs. 14a and 15a), and fit the sparse D data reasonably well, with the exception of the D LREE, which are higher than values predicted by the LSM (Fig. 9).

The observation of a plateau effect for the extremely incompatible elements (La, Ce, Nd; Figs. 13 and 15) in most natural and some experimental partitioning studies suggests that effective D values for other extremely incompatible elements (Cs, K, Rb, Ba, Th, Nb) may also be higher than they should if full equilibrium were to have prevailed. Perhaps the cooling and crystallization rates in natural magmatic systems are sufficiently high that equilibrium partitioning is the exception, rather than the rule, and the effective D values bottom out for kinetic reasons? In terms of modeling, this suggests that different strategies may pertain to different petrogenetic scenarios. If the process to be simulated is melting of a slowly upwelling mantle diapir, or a slowly cooled layered intrusion (<500 °C/hr) then values of D La–Ce–Nd–Sm calculated with the LSM would apply. If one wishes to model intra-crustal fractional crystallization of a fast-cooling magma sheet, or any process where timescales are short, then a constant D LREE value=D Sm may be more germane. Alternatively, if Kennedy et al. (1993) and Beattie (1994) are correct in attributing the LREE plateau effect to incorporation of a small amount of trapped melt (ca. 0.3% to 1%) in the growing crystal, then an effective D value could be calculated simply by incorporating the effects of a trapped melt fraction.

$$D_e = (D(1-a)) + a \quad (2)$$

where D_e=D effective, and a=the fraction of trapped melt with D=1 (e.g., see Bédard, 2001).

It has been suggested that ${}^{\text{olivine/liquid}}D_{\text{HFSC}} > {}^{\text{olivine/liquid}}D_{\text{REE}}$ (HFSC=High Field Strength Cations, REE=Rare Earth Elements), and that melts percolating through the mantle that assimilate orthopyroxene and crystallize olivine acquire 'arc'-like geochemical signatures as a result (Kelemen et al., 1990). The ubiquitous presence of positive D Ti and D Ta anomalies for all mafic–ultramafic melt compositions, and of positive D Zr and D Hf anomalies for basaltic compositions (Fig. 15), suggests that crystallization of

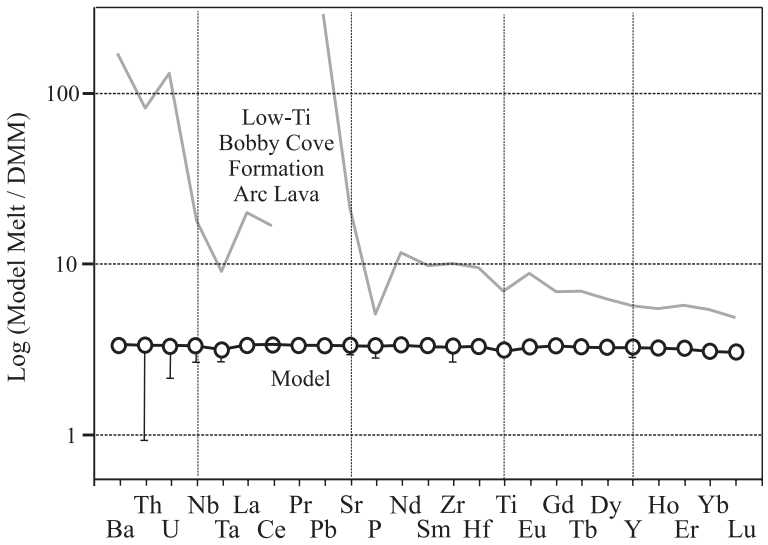

Fig. 16. Model melt derived from a mid-ocean ridge basalt source (DMM from Bédard, 1999; Workman and Hart, submitted for publication) through 30% equilibrium melting (C_L=C_o/(D+F(1−D)), C_L=concentration in the liquid, C_o=concentration in the source, F=melt fraction) with a dunitic residue and 10 wt.% MgO in the melt. Error bars are values from the regressions against melt MgO (Table 2). No error bars are shown for Ta and Pr because these elements were not regressed. Symbols are generally larger than errors. Typical Arc melt from Bédard et al. (2000).

olivine, or decompressive melt-rock reactions involving precipitation of olivine, could perhaps generate perceptible negative anomalies for Ta, Ti, Zr and Hf. The general absence of a positive D Nb anomaly, on the other hand (Fig. 15), seems inconsistent with generation of a true 'arc' signature as a result of such a process. As an example, Fig. 16 shows the composition of a 10% MgO melt formed by 30% equilibrium melting of fertile MORB mantle (DMM) with a dunitic residue (Bédard, 1999). The error bars represent the uncertainties resulting solely from the regressions of D from Table 2. The MORB-normalized model melt has a flat profile, with only weak HFSC anomalies, very different from typical arc-type magmas (Fig. 16).

6. Conclusions

Nernst partition coefficient data between olivine and silicate melt ($^{\text{olivine/liquid}}D$) show significant variability for many trace elements of petrological interest. Variations of $^{\text{olivine/liquid}}D$ are parameterized against the MgO wt.% of the melt, and typically show trends of increasing D with decreasing MgO. Comparisons of the $^{\text{olivine/liquid}}D$ regressions to results of the Lattice Strain Model (LSM) yield well-constrained relationships between liquid MgO, D_0, E_M^{3+}, with constant r_0, allowing $^{\text{olivine/liquid}}D$ REE–Y–Sc to be calculated with the LSM for any MgO content (Tables 2 and 3). The parameterizations proposed here should provide improved solutions to trace element models applied to olivine-bearing systems. The D data suggest that basaltic melts in equilibrium with olivine may acquire weak negative Hf–Zr–Ti–Ta anomalies, but that negative Nb anomalies are unlikely to develop. The misfits between results of the Lattice Strain Model and most LREE and LILE partitioning data suggest that kinetic effects may limit the lower value of D for extremely incompatible elements in natural situations characterized by high cooling/crystallization rates.

Acknowledgments

Jon Blundy helped with the calculation of the Lattice Strain Model. My aching fingers and I wish to thank Steve Parman, Laura Wasylenki, Linda Elkins-Tanton, Jasper Berndt, Trevor Green, John Adam and Bruno Scaillet, who contributed their datasets. The ms benefitted from the constructive comments of Chusi Li and Roger Nielsen. This is Geological Survey of Canada Contribution # 2004105.

Appendix A. Supplementary data

Supplementary data associated with this article can be found, in the online version, at doi:10.1016/j.lithos.2005.03.011.

References

Arndt, N.T., 1977. Partitioning of nickel between olivine and ultrabasic and basic komatiite liquids. Year B.-Carnegie Inst. Wash. 76, 553–557.

Baker, D.R., Eggler, D.H., 1987. Compositions of anhydrous melts coexisting with plagioclase, augite and olivine or low-Ca pyroxene from 1 atm to 8 kbar: application to the Aleutian volcanic center of Atka. Am. Mineral. 72, 12–28.

Baker, M.B., Stolper, E.M., 1994. Determining the composition of high-pressure mantle melts using diamond aggregates. Geochim. Cosmochim. Acta 58, 2811–2827.

Barker, F., Wones, D.R., Sharp, W.N., Desborough, G.A., 1975. The Pikes Peak Batholith, Colorado Front Range, and a model for the origin of the gabbro–anorthosite–syenite–potassic granite suite. J. Prec. Res. 2, 97–160.

Barnes, S.J., 1986. The effect of trapped liquid crystallization on cumulus mineral compositions in layered intrusions. Contrib. Mineral. Petrol. 93, 524–531.

Barrat, J.A., Jambon, A., Bohn, M., Gillet, P., Sautter, V., Gopel, C., Lesourd, M., Keller, F., 2002. Petrology and chemistry of the picritic shergottite North West Africa 1068 (NWA 1068). Geochim. Cosmochim. Acta 66, 3505–3518.

Beattie, P., 1993. The generation of Uranium series disequilibria by partial melting of spinel peridotite: constraints from partitioning studies. Earth Planet. Sci. Lett. 117, 379–391.

Beattie, P., 1994. Systematics and energetics of trace-element partitioning between olivine and silicate melts: implications for the nature of mineral/melt partitioning. Chem. Geol. 117, 57–71.

Beattie, P., Ford, C., Russell, D., 1991. Partition coefficients for olivine–melt and orthopyroxene–melt systems. Contrib. Mineral. Petrol. 109, 212–224.

Bédard, J.H., 1994. A procedure for calculating the equilibrium distribution of trace elements among the minerals of cumulate rocks, and the concentration of trace elements in the coexisting liquids. Chem. Geol. 118, 143–153.

Bédard, J.H., 1999. Petrogenesis of boninites from the Betts Cove Ophiolite, Newfoundland, Canada: identification of subducted source components. J. Petrol. 40, 1853–1889.

Bédard, J.H., 2001. Parental magmas of Nain Plutonic Suite anorthosites and mafic cumulates: a trace element modelling approach. Contrib. Mineral. Petrol. 141, 747–771.

Bédard, J.H., Hébert, R., 1998. Formation of chromitites by assimilation of crustal pyroxenites and gabbros into peridotitic intrusions: North Arm Mountain massif, Bay of Islands ophiolite, Newfoundland, Canada. J. Geophys. Res. 103, 5165–5184.

Bédard, J.H., Ludden, J., Francis, D., 1987. The Mégantic intrusive complex of Québec: a study of the derivation of silica oversaturated anorogenic magmas of alkaline affinity. J. Petrol. 28, 355–388.

Bédard, J.H., Lauzière, K., Tremblay, A., Sangster, A., Dec, T., 2000. The Betts Cove Ophiolite and its cover rocks, Newfoundland. Bull.-Geol. Surv. Can. 550 (76 pp.).

Berndt, J., 2002. Differentiation of MOR basalt at 200 MPa: experimental techniques and influence of H_2O and f_{O_2} on phase relations and liquid line of descent. PhD Dissert., Universität Hannover, Germany. 118 pp.

Blatter, D.L., Carmichael, I.S.E., 2001. Hydrous phase equilibria of a Mexican high-silica andesite: a candidate for a mantle origin? Geochim. Cosmochim. Acta 65, 4043–4065.

Blundy, J.D., Wood, B.J., 1991. Crystal-chemical controls on the partitioning of Sr and Ba between plagioclase feldspar, silicate melts, and hydrothermal solutions. Geochim. Cosmochim. Acta 55, 193–209.

Blundy, J.D., Wood, B.J., 1994a. Prediction of crystal–melt partition coefficients from elastic moduli. Nature 372, 452–454.

Blundy, J.D., Wood, B.J., 1994b. Crystal-chemical controls on the partitioning of Sr and Ba between plagioclase feldspar, silicate melts, and hydrothermal solutions. Geochim. Cosmochim. Acta 55, 193–209.

Blundy, J., Wood, B.J., 2003. Partitioning of trace elements between crystals and melts. Earth Planet. Sci. Lett. 210, 383–397.

Blundy, J.D., Wood, B.J., Davies, A., 1996. Thermodynamics of rare earth element partitioning between clinopyroxene and melt in the system $CaO–MgO–Al_2O_3–SiO_2$. Geochim. Cosmochim. Acta 60, 359–364.

Bodinier, J.-L., Vasseur, G., Vernières, J., Dupuy, C., Fabriès, J., 1990. Mechanism of mantle metasomatism: geochemical evidence from the Lherz orogenic peridotite. J. Petrol. 31, 597–628.

Brenan, J.M., McDonough, W.F., Dalpé, C., 2003. Experimental constraints on the partitioning of rhenium and some platinum-group elements between olivine and silicate melt. Earth Planet. Sci. Lett. 212, 135–150.

Brice, J.C., 1975. Some thermodynamic aspects of the growth of strained crystals. J. Cryst. Growth 28, 249–253.

Brown, G.E., 1982. Olivines and silicate spinels. In: Ribbe, P.H. (Ed.), Orthosilicates, Reviews in Mineralogy, vol. 5. Mineral. Soc. Amer., pp. 275–381.

Brunet, F., Chazot, G., 2001. Partitioning of phosphorus between olivine, clinopyroxene and silicate glass in a spinel lherzolite xenolith from Yemen. Chem. Geol. 176, 51–72.

Burton, K.W., Gannoun, A., Birck, J.L., Allègre, C.J., Schiano, P., Clocchiatti, R., Alard, O., 2002. The compatibility of rhenium and osmium in natural olivine and their behaviour during mantle melting and basalt genesis. Earth Planet. Sci. Lett. 198, 63–76.

Canil, D., 1997. Vanadium partitioning and the oxidation state of Archaean komatiite magmas. Nature 389, 842–845.

Canil, D., Fedortchouk, Y., 2001. Olivine–liquid partitioning of vanadium and other trace elements, with applications to modern and ancient picrites. Can. Mineral. 39, 319–330.

Capobianco, C.J., Drake, M.J., Rogers, P.S.Z., 1991. Crystal/melt partitioning of Ru, Rh and Pd for silicate and oxide phases. Lunar Planet. Sci. Inst. 22, 179–180 (abstract).

Carmichael, I.S.E., Nicholls, J., Smith, A.L., 1970. Silica activity in igneous rocks. Am. Mineral. 55, 246–263.

Cawthorn, R.G., 1996. Layered intrusions. In: Cawthorn, R.G. (Ed.), Dev. in Petrol., vol. 15. Elsevier Science Publ. B. V. 531 pp. and map.

Colson, R.O., McKay, G.A., Taylor, R.A., 1988. Temperature and composition dependencies of trace element partitioning: olivine/melt and low-Ca pyroxene melt. Geochim. Cosmochim. Acta 52, 539–553.

Colson, R.O., Colson, M.C., Nermoe, M.K.B., Floden, A.M., Hendrickson, T.R., 2000. Effects of aluminum on Cr dimerization in silicate melts and implications for Cr partitioning and redox equilibria. Geochim. Cosmochim. Acta 64, 527–543.

Dilek, Y., Robinson, P.T. (Eds.), 2003. Ophiolites in Earth History, Spec. Publ. 218, Geol. Soc. London vii, 717 pp.

Dostal, J., Capedri, S., 1975. Partition coefficients of Uranium for some rock-forming minerals. Chem. Geol. 15, 285–294.

Dostal, J., Dupuy, C., Carron, J.P., LeGuen de Kerneizon, M., Maury, R.C., 1983. Partition coefficients of trace elements: application to volcanic rocks of St. Vincent, West Indies. Geochim. Cosmochim. Acta 47, 525–533.

Duke, J.M., 1976. Distribution of the period four transition elements among olivine, calcic clinopyroxene and mafic silicate liquid: experimental results. J. Petrol. 17, 499–521.

Dunn, T., 1987. Partitioning of Hf, Lu, Ti, and Mn between olivine, clinopyroxene and basaltic liquid. Contrib. Mineral. Petrol. 96, 476–484.

Dunn, T., Sen, C., 1994. Mineral/matrix partition coefficients for orthopyroxene, plagioclase, and olivine in basaltic to andesitic systems: a combined analytical and experimental study. Geochim. Cosmochim. Acta 58, 717–733.

Elkins-Tanton, L.T., Grove, T.L., 2003. Evidence for deep melting of hydrous metasomatized mantle: Pliocene high-potassium magmas from the Sierra Nevadas. J. Geophys. Res. 108, (art.# 2350).

Elkins-Tanton, L.T., Fernandes, V.A., Delano, J.W., Grove, T.L., 2000. Origin of lunar ultramafic green glasses: constraints from phase equilibtrium studies. Geochim. Cosmochim. Acta 64, 2339–2350.

Elkins-Tanton, L.T., Chatterjee, N., Grove, T.L., 2003. Experimental and petrological constraints on lunar differentiation from the Apollo 15 green picritic glasses. Meteorit. Planet. Sci. 38, 515–527.

Francalanci, L., 1989. Trace element partitioning coefficients for minerals in shoshonitic and calc-alkaline rocks from Stromboli Island (Aeolian Arc). Neues Jahrb. Mineral. Abh. 160, 229–247.

Fujimaki, H., Tatsumoto, M., Aoki, K., 1984. Partition coefficients of Hf, Zr and REE between phenocrysts and groundmass. Proc.

14th Lunar and Planet. Sci. Conf. Part 2. J. Geophys. Res., vol. 89, pp. B662–B672. Supplement.
Gaetani, G.A., Grove, T.L., 1995. Partitioning of rare earth elements between clinopyroxene and silicate melt: crystal-chemical controls. Geochim. Cosmochim. Acta 59, 1951–1962.
Gaetani, G.A., Grove, T.L., 1998. The influence of water on melting of mantle peridotite. Contrib. Mineral. Petrol. 131, 323–346.
Grove, T.L., Juster, T.C., 1989. Experimental investigations of low-Ca pyroxene stability and olivine–pyroxene–liquid equilibria at 1-atm in natural basaltic and andesitic liquids. Contrib. Mineral. Petrol. 103, 287–305.
Grove, T.L., Gerlach, D.C., Sando, T.W., 1982. Origin of calc-alkaline series lavas at Medicine Lake volcano by fractionation, assimilation and mixing. Contrib. Mineral. Petrol. 80, 160–182.
Grove, T.L., Elkins-Tanton, L.T., Parman, S.W., Chatterjee, N., Münterer, O., Gaetani, G., 2003. Fractional crystallization and mantle-melting controls on calc-alkaline differentiation trends. Contrib. Mineral. Petrol. 145, 515–533.
Hanson, B., Jones, J.H., 1998. The systematics of Cr^{3+} and Cr^{2+} partitioning between olivine and liquid in the presence of spinel. Am. Mineral. 83, 669–684.
Hart, S.R., Davis, K.E., 1978. Nickel partitioning between olivine and silicate melt. Earth Planet. Sci. Lett. 40, 203–219.
Herzberg, C., Zhang, J., 1996. Melting experiments on anhydrous peridotite KLB-1: compositions of magmas in the upper mantle and transition zone. J. Geophys. Res. 101, 8271–8295.
Hesse, M., Grove, T.L., 2003. Absarokites from the western Mexican Volcanic Belt: constraints on mantle wedge conditions. Contrib. Mineral. Petrol. 146, 10–27.
Hill, E., Wood, B.J., Blundy, J.D., 2000. The effect of Ca-Tschermaks component on trace element partitioning between clinopyroxene and silicate melt. Lithos 53, 203–215.
Hofmann, A.W., 1988. Chemical differentiation of the Earth: the relationship between mantle, continental crust, and oceanic crust. Earth Planet. Sci. Lett. 90, 297–314.
Hsu, W.B., 2003. Minor element zoning and trace element geochemistry of pallasites. Meteorit. Planet. Sci. 38, 1217–1241.
Karner, J., Papike, J.J., Shearer, C.K., 2003. Olivine from planetary basalts: chemical signatures that indicate planetary parentage and those that record igneous setting and process. Am. Mineral. 88, 806–816.
Kelemen, P.B., Johnson, K.T.M., Kinzler, R.J., Irving, A.J., 1990. High-field-strength element depletions in arc basalts due to mantle–magma interaction. Nature 345, 521–524.
Kennedy, A.K., Lofgren, G.E., Wasserburg, G.J., 1993. An experimental study of trace element partitioning between olivine, orthopyroxene and melt in chondrules: equilibrium values and kinetic effects. Earth Planet. Sci. Lett. 115, 177–195.
Kinzler, R.J., 1997. Melting of mantle peridotite at pressures approaching the spinel to garnet transition: application to mid-ocean ridge basalt petrogenesis. J. Geophys. Res. 102, 853–874.
Kinzler, R.J., Grove, T.L., 1992. Primary magmas of mid-ocean ridge basalts: 1. Experiments and methods. J. Geophys. Res. 97, 6885–6906.
Kinzler, R.J., Grove, T.L., Recca, S.I., 1990. An experimental study on the effect of temperature and melt composition on the partitioning of nickel between olivine and silicate melt. Geochim. Cosmochim. Acta 54, 1255–1265.
Kohn, S.C., Schofield, P.F., 1994. The importance of melt composition in controlling trace-element behaviour: an experimental study of Mn and Zn partitioning between forsterite and silicate melts. Chem. Geol. 117, 73–87.
Langmuir, C.H., 1989. Geochemical consequences of in situ crystallization. Nature 340, 199–205.
Laporte, D., Toplis, M.J., Seyler, M., Devidal, J.L., 2004. A new experimental technique for extracting liquids from peridotite at very low degrees of meltingapplication to partial melting of depleted peridotite. Contrib. Mineral. Petrol. 146, 463–484.
Larsen, L.-M., 1979. Distribution of REE and other trace elements between phenocrysts and peralkaline undersaturated magmas ecemplified by rocks from the Gardar igneous province, south Greenland. Lithos 12, 303–315.
LeMarchand, F., Villemant, B., Calas, G., 1987. Trace element distribution coefficients in alkaline series. Geochim. Cosmochim. Acta 51, 1071–1081.
Li, C., Maier, W.D., de Waal, S.A., 2001. Magmatic N–Cu versus PGE deposits: contrasting genetic controls and exploration implication. S. Afr. J. Geol. 188, 149–159.
Li, C., Ripley, E.M., Mathez, E.A., 2003. The effect of S on the partitioning of Ni between olivine and silicate melt in MORB. Chem. Geol. 201, 295–306.
Longhi, J., 1995. Liquidus equilibria of some primary lunar and terrestrial melts in the garnet stability field. Geochim. Cosmochim. Acta 59, 2375–2386.
Longhi, J., 2002. Some phase equilibrium systematics of lherzolite melting I. Geochem. Geophys. Geosyst. (G^3) 3 (3).
Longhi, J., Van der Auwera, J., Fram, M.S., Duchesne, J.C., 1999. Some phase equilibrium constraints on the origin of Proterozoic (Massif) anorthosites and related rocks. J. Petrol. 40, 339–362.
Loucks, R.R., 1996. Restoration of the elemental and stable-isotopic compositions of diffusionally altered minerals in slowly cooled rocks. Contrib. Mineral. Petrol. 124, 346–358.
Luhr, J.F., Carmichael, I.S.E., 1980. The Colima volcanic complex, Mexico: I. Post-caldera andesites from Volcan Colima. Contrib. Mineral. Petrol. 71, 343–372.
Maclennan, J., McKenzie, D., Grönvold, K., Shimizu, N., Eiler, J.M., Kitchen, N., 2003. Melt mixing and crystallization under Theistareykir, northeast Iceland. Geochem. Geophys. Geosyst. (G^3) 4 (art. 8624).
Mahood, G.A., Hildreth, W., 1983. Large partition coefficients for elements in high-silica rhyolites. Geochim. Cosmochim. Acta 47, 11–30.
Mahood, G.A., Stimac, J.A., 1990. Trace-element partitioning in pantellerites and trachytes. Geochim. Cosmochim. Acta 54, 2257–2276.
McDade, P., Blundy, J.D., Wood, B.J., 2003. Trace element partitioning on the Tinaquillo Lherzolite solidus at 1.5 GPa. Phys. Earth Planet. Inter. 139, 129–147.
McDonough, W.F., Stosch, H.G., Ware, N.G., 1992. Distribution of titanium and the rare earth elements between peridotitic minerals. Contrib. Mineral. Petrol. 110, 321–328.

McKay, G.A., 1986. Crystal/liquid partitioning of REE in basaltic systems: extreme fractionation of REE in olivine. Geochim. Cosmochim. Acta 50, 69–79.

Michael, P.J., 1988. Partition coefficients for rare earth elements in mafic minerals of high silica rhyolites: the importance of accessory mineral inclusions. Geochim. Cosmochim. Acta 52, 275–282.

Moore, G.M., Carmichael, I.S.E., 1998. The hydrous phase equilibria (to 3 kbar) of an andesite and basaltic andesite from western Mexico: constraints on water content and conditions of phenocryst growth. Contrib. Mineral. Petrol. 130, 304–319.

Mysen, B.O., 1978. Experimental determination of rare earth element partitioning between hydrous silicate melt, amphibole, and garnet peridotite minerals at upper mantle pressures and temperatures. Geochim. Cosmochim. Acta 42, 1253–1263.

Mysen, B.O., 1983. The structure of silicate melts. Annu. Rev. Earth Planet. Sci. 11, 75–97.

Mysen, B.O., Virgo, D., 1980. Trace element partitioning and melt structure: an experimental study at 1 atm pressure. Geochim. Cosmochim. Acta 44, 1917–1930.

Nekvasil, H., Dondolini, A., Horn, J., Filberto, J., Long, H., Lindsley, D.H., 2004. The origin and evolution of silica-saturated alkalic suites: an experimental study. J. Petrol. 45, 693–721.

Nielsen, R.L., 1985. A method for the elimination of the compositional dependence of trace element distribution coefficients. Geochim. Cosmochim. Acta 49, 1775–1779.

Nielsen, R.L., Drake, M.J., 1979. Pyroxene–melt equilibria. Geochim. Cosmochim. Acta 43, 1259–1272.

Nielsen, R.L., Gallahan, W.E., Newberger, F., 1992. Experimentally determined mineral–melt partition coefficients for Sc, Y and REE for olivine, orthopyroxene, pigeonite, magnetite and ilmenite. Contrib. Mineral. Petrol. 110, 488–499.

Niu, Y.L., Regelous, M., Wendt, I.J., Batiza, R., O'Hara, M.J., 2002. Geochemistry of near-EPR seamounts: importance of source vs. process and the origin of enriched mantle component. Earth Planet. Sci. Lett. 199, 327–345.

Nixon, P.H., 1987. Mantle Xenoliths. John Wiley and Sons, New York. 844 pp.

O'Hara, M.J., 1977. Geochemical evolution during fractionation crystallization of a periodically refilled magma chamber. Nature 266, 503–507.

O'Hara, M.J., 1995. Trace element geochemical effects of integrated melt extraction and 'shaped' melting regimes. J. Petrol. 36, 1111–1132.

O'Neill, H.S.C., Eggins, S.M., 2002. The effect of melt composition on trace element partitioning: an experimental investigation of the activity coefficients of FeO, NiO, CoO, MoO_2 and MoO_3 in silicate melts. Chem. Geol. 186, 151–181.

Onuma, N., Higuchi, H., Wakita, H., Nagasawa, H., 1968. Trace element partitioning between two pyroxenes and the host lava. Earth Planet. Sci. Lett. 5, 47–51.

Parman, S.W., Grove, T.L., 2004. Harzburgite melting with and without H_2O: experimental data and predictive modeling. J. Geophys. Res. 109 (Article number B02201).

Parman, S.W., Dann, J.C., Grove, T.L., deWit, M.J., 1997. Emplacement conditions of komatiite magmas from the 3.49 Ga Komati Formation, Barberton Greenstone Belt, South Africa. Earth Planet. Sci. Lett. 150, 303–323.

Pickering-Witter, J., Johnston, A.D., 2000. The effects of variable bulk composition on the melting systematics of fertile peridotitic assemblages. Contrib. Mineral. Petrol. 140, 190–211.

Puchtel, I.S., Humayun, M., Campbell, A.J., Sproule, R.A., Lesher, C.M., 2004. Platinum group element geochemistry of komatiites from the Alexo and Pyke hill areas, Ontario, Canada. Geochim. Cosmochim. Acta 68, 1361–1383.

Purton, J.A., Blundy, J.D., Allan, N.L., 2000. Computer simulation of high-temperature forsterite–melt partitioning. Am. Mineral. 85, 1087–1091.

Righter, K., Carmichael, I.S.E., 1996. Phase equilibria of phlogopite lamprophyres from western Mexico: biotite–liquid equilibria and *P–T* estimates for biotite-bearing igneous rocks. Contrib. Mineral. Petrol. 123, 1–21.

Righter, K., Campbell, A.J., Humayun, M., Hervig, R.L., 2004. Partitioning of Ru, Rh, Pd, Re, Ir, and Au between Cr-bearing spinel, olivine, pyroxene and silicate melts. Geochim. Cosmochim. Acta 68, 867–880.

Roeder, P.L., Emslie, R.F., 1970. Olivine–liquid equilibrium. Contrib. Mineral. Petrol. 29, 275–289.

Scaillet, B., MacDonald, R., 2001. Phase relations of peralkaline silicic magmas and petrogenetic interpretations. J. Petrol. 42, 825–845.

Schmidt, M.W., Green, D.H., Hibberson, W.O., 2004. Ultra-calcic magmas generated from Ca-depleted mantle: an experimental study on the origin of ankaramites. J. Petrol. 45, 531–554.

Schnetzler, C.C., Philpotts, J.A., 1970. Partition coefficients of rare-earth elements between igneous matrix material and rock-forming mineral phenocrysts II. Geochim. Cosmochim. Acta 34, 331–340.

Schreiber, H.D., Haskin, L.A., 1976. Chromium in basalts: experimental determination of redox states and partitioning among synthetic silicate phases. Proc. 7th Lunar Planet. Sci. Conf., pp. 1221–1259.

Schwab, B.E., Johnson, A.D., 2001. Melting systematics of modally variable, compositionally intermediate peridotites and the effect of mineral fertility. J. Petrol. 42, 1789–1811.

Shannon, R.D., 1976. Revised effective ionic raii and systematic studies of interatomic distances in halides and chalcogenides. Acta Crystallogr., A 32, 751–767.

Shaw, D.M., 1970. Trace element fractionation during anatexis. Geochim. Cosmochim. Acta 34, 237–243.

Shaw, D.M., 2000. Continuous (Dynamic) melting theory revisited. Can. Mineral. 38, 1041–1063.

Shimizu, H., Sangen, K., Masuda, A., 1982. Experimental study on rare-earth element partitioning in olivine and clinopyroxene formed at 10 and 20 kb for basaltic systems. Geochem. J. 16, 107–117.

Spera, F.J., Bohrson, W.A., 2002. Energy-constrained open-system magmatic processes: 3. Energy-constrained recharge, assimilation, and fractional crystallization (EC-RAFC). Geochem. Geophys. Geosyst. (G^3) 3 (art. # 8001).

Sugawara, T., 2000. Empirical relationships between temperature, pressure, and MgO content in olivine and pyroxene saturated liquid. J. Geophys. Res. 105, 8457–8472.

Suzuki, T., Akaogi, M., 1995. Element partitioning between olivine and silicate melt under high pressure. Phys. Chem. Miner. 22, 411–418.

Sweeney, R.J., Prozesky, V., Przybylowicz, W., 1995. Selected trace and minor element partitioning between peridotite minerals and carbonatite melts at 18–46 kb pressure. Geochim. Cosmochim. Acta 59, 3671–3683.

Thompson, R.N., Morrison, M.A., Dickin, A.P., Hendry, G.L., 1983. Continental flood basalts... Arachnids rule OK? In: Hawkesworth, C.J., Norry, M.J. (Eds.), Continental Basalts and Mantle Xenoliths. Shiva Publishing Ltd., Cheshire, U.K., pp. 158–185.

Toplis, M.J., Carroll, M.R., 1996. Differentiation of ferro-basaltic magmas under conditions open and closed to oxygen: implications for the Skaergaard intrusion and other natural systems. J. Petrol. 37, 837–858.

Toplis, M.J., Libourel, G., Carroll, M.R., 1994. The role of phosphorus in crystallisation processes of basalt: an experimental study. Geochim. Cosmochim. Acta 58, 797–810.

Villemant, B., Joron, J.L., Jaffrezic, H., Treuil, M., Maury, R.C., Brousse, R., 1980. Cristallisation fractionnée d'un magma basaltique alcalin: la série de la Chaîne des Puys (Massif Central, France). III: Géochimie. Bull. Minéral. 103, 267–286.

Walter, M.J., 1998. Melting of garnet peridotite and the origin of komatiite and depleted lithosphere. J. Petrol. 39, 29–60.

Wasylenki, L.E., Baker, M.B., Kent, A.J.R., Stolper, E.M., 2003. Near-solidus melting of the shallow upper mantle: partial melting experiments on depleted peridotite. J. Petrol. 44, 1163–1191.

Weyer, S., Munker, C., Mezger, K., 2003. Nb/Ta, Zr/Hf and REE in the depleted mantle: implications for the differentiation history of the crust–mantle system. Earth Planet. Sci. Lett. 205, 309–324.

Wood, B.J., Blundy, J.D., 1997. A predictive model for rare earth element partitioning between clinopyroxene and anhydrous silicate melt. Contrib. Mineral. Petrol. 129, 166–181.

Wood, B.J., Blundy, J.D., 2002. The effect of H_2O on crystal–melt partitioning of trace elements. Geochim. Cosmochim. Acta 66, 3647–3656.

Workman, R.K., Hart, S.R., submitted for publication. Major and trace element composition of the depleted MORB mantle (DMM). Earth Planet. Sci. Lett.

Wörner, G., Beusen, J.-M., Duchateau, N., Gijbels, R., Schmincke, H.-U., 1983. Trace element abundances and mineral/melt distribution coefficients in phonolites from the Laacher See Volcano (Germany). Contrib. Mineral. Petrol. 84, 152–173.

Yang, H.J., Kinzler, R.J., Grove, T.L., 1996. Experiments and models of anhydrous, basaltic olivine–plagioclase–augite saturated melts from 0.001 to 10 kbar. Contrib. Mineral. Petrol. 124, 1–18.